Unified View of Sediment Transport by Currents and Waves. II: Suspended Transport

Leo C. van Rijn[1]

Abstract: The problem of suspended sediment transport in river and coastal flows is addressed. High-quality field data of river and coastal flows have been selected and clustered into four particle size classes (60–100, 100–200, 200–400, and 400–600 μm). The suspended sand transport is found to be strongly dependent on particle size and on current velocity. The suspended sand transport in the coastal zone is found to be strongly dependent on the relative wave height (H_s/h), particularly for current velocities in the range 0.2–0.5 m/s. The time-averaged (over the wave period) advection–diffusion equation is applied to compute the time-averaged sand concentration profile for combined current and wave conditions. Flocculation, hindered settling, and stratification effects are included by fairly simple expressions. The bed-shear stress is based on a new bed roughness predictor. The reference concentration function has been recalibrated using laboratory and field data for combined steady and oscillatory flow. The computed transport rates show reasonably good agreement (within a factor of 2) with measured values for velocities in the range of 0.6–1.8 m/s and sediments in the range of 60–600 μm. The proposed method underpredicts in the low-velocity range (<0.6 m/s). A new simplified transport formula is presented, which can be used to obtain a quick estimate of suspended transport. The modeling of wash load transport in river flow based on the energy concept of Bagnold shows that an extremely large amount of very fine sediment (clay and very fine silt) can be transported by the flow.

DOI: 10.1061/(ASCE)0733-9429(2007)133:6(668)

CE Database subject headings: Sediment transport; Suspended sediments; Currents; Waves; Rivers; Coastal environment.

Introduction

Generally, suspended transport is the dominant mode of transport in the lower reaches of rivers, in tidal rivers, and along sandy beaches where fine sediment beds prevail. The sediment beds are classified into subclasses, using the following class separation diameters: d_{gravel}=2,000 μm, d_{sand}=62 μm, d_{silt}=32 μm, and d_{cs}=8 μm. A high-quality field data set of suspended transport rates in rivers and coastal waters is established and analyzed herein to reveal the basic influence of the flow regime (velocity, wave height) and the sediment particle size. The most common approach to model the suspended sediment transport is based on the advection–diffusion theory representing the downward transport by gravity (settling) and the upward transport by turbulent processes (mixing), resulting in a Rouse-type sediment concentration profile over the water depth. Using this approach, the writer (van Rijn 1984a,b,c, 1993, 2005, 2007) presented a prediction method for steady river flow. This method is generalized by including a bed roughness predictor and extended to the coastal flow regime by including wave-related mixing processes and by recalibrating the reference concentration using laboratory and field data of combined steady and oscillatory flow (current plus waves). Special attention is given to modeling of sediment concentration and transport in the fine silt and sand range using data sets from the Huanghe River and the Yangtze Estuary in China, where flocculation and hindered settling effects are of crucial importance. The new general prediction method (TR2004 model) is severely tested against field data of river and coastal flows, showing reasonably good results. The method is universal in the sense that it can be applied to the full size range of 8–2,000 μm and the full hydrodynamic regime of quasi-steady river and tidal flow and coastal flow. A new simplified transport formula is presented, which can be used to obtain a quick estimate of suspended transport in river and coastal flows. Finally, the modeling of wash load transport in river flow is addressed using the energy concept of Bagnold (1962, 1966). Using this approach, it can be shown that an extremely large amount (up to 1,000 kg/m^3) of very fine sediment can be transported by the flow.

Analysis of Suspended Transport Data

River and Tidal Flow Conditions (Current Only)

The most basic case is suspended transport by a current without waves (river and tidal flow). Quasi-steady tidal flows are different from river flow as regards bed forms and bed roughness. Large dune-type bed forms will generally not be generated by tidal flow. Often, the bed forms are not in equilibrium with the flow velocity and can even have a reversed asymmetry. High-quality field data sets (340) from major rivers and estuaries around the world available in the literature (see Table 1) have been analyzed to study the relationship between suspended sand transport, current

[1]Senior Engineer, Delft Hydraulics, P.O. Box 177, Delft 2600 MH, The Netherlands; and, Professor, Univ. of Utrecht, P.O. Box 80115, Utrecht 3508TC, The Netherlands.

Note. Discussion open until November 1, 2007. Separate discussions must be submitted for individual papers. To extend the closing date by one month, a written request must be filed with the ASCE Managing Editor. The manuscript for this paper was submitted for review and possible publication on July 8, 2005; approved on August 2, 2006. This paper is part of the ***Journal of Hydraulic Engineering***, Vol. 133, No. 6, June 1, 2007. ©ASCE, ISSN 0733-9429/2007/6-668–689/$25.00.

Table 1. Summary of Field Data of Suspended Transport for River and Tidal Flow

Source		Number of cases	Number of groups	Sediment size d_{50} (μm)	Water depth h (m)	Depth/mean velocity u (m/s)	Bed forms
Location	Reference						
Mississippi River, U.S.	Peterson and Howels (1973) Scott and Stephens (1966)	103	26	150–400	1–15	0.6–2.2	NM
Huanghe River, China	Van den Berg and Van Gelder (1993)	13	7	60–100	1–4	0.45–1.85	F/R
Rio Grande River, U.S.	Culbertson et al. (1972)	20	5	180–230	1–2	1.2–2	NM
Nile River, Egypt	Abdel-Fattah (1997)	54	15	250–600	4–6	0.3–0.9	D/R
Rhine River, The Netherlands	Kleinhans (1999)	10	4	2,500–3,000	9–11	1.4–2	D
Galgeplaat, eastern Scheldt, The Netherlands	van Rijn et al. (2001)	5	5	150	2–4	0.2–0.6	R
Eastern and western Scheldt Estuaries, The Netherlands	Voogt et al. (1991)	85	27	180–320	4–11	1.3–2.2	D/R
Foulness, Outer Thames Estuary, U.K.	Whitehouse et al. (1997)	26	6	120–180	14–16	0.3–1.2	R/F
Maplin Sands, U.K.	Whitehouse et al. (1996)	24	5	110–170	4–6	0.3–0.7	R/F

Note: h=water depth; u=depth-averaged current velocity; NM=not measured; R=ripples; D=dunes; and F=flat bed.

velocity, water depth, and sand diameter. Only data sets with water depths larger than 1 m have been selected. The particle size range is 60–2300 μm. The depth-averaged current velocity range is 0.3–2.2 m/s. Individual data points have been clustered as much as possible into data groups of water depth and current velocity to reduce the scatter. The data points within the groups have been averaged to obtain representative values. The variation range of the water depth within a group is about 10% of the mean value; the variation range of the current velocity is 10–25%; the variation range of the corresponding suspended transport rates is as large as 50%.

Figs. 1–4 show the suspended sand transport rates (including variation ranges) as a function of depth-averaged velocity for four sand diameter classes (60–100, 100–200, 200–400, and 400–600 μm). Analysis of the results shows that the effect of water depth (between 1 and 15 m) on the suspended sand transport is of minor importance. The suspended sand transport is dominantly dependent on the current velocity; the transport increases by a factor of about 500 for velocities increasing from 0.4 to 2 m/s. Empirical trend lines of suspended sand transport against velocity are also shown in Figs. 1–4 and are summarized in Fig. 5.

The empirical trend lines can be roughly approximated by

$$q_s = (d_{\text{ref}}/d_{50})^2(u - u_{\text{cr}})^3 \quad (1)$$

with: q_s=suspended transport (kg/s/m); d_{50}=median grain size (m); d_{ref}=reference grain size=0.0003 m; u=depth-averaged velocity (m/s); and u_{cr}=critical depth-averaged velocity =0.25 (m/s). Hence, the suspended transport is inversely proportional to the square of the grain size. The empirical trend line of the bed-load transport in the range of 200–1000 μm (most of the data are in the range of 400–1000 μm) is also shown in Fig. 5.

The bed-load transport is significantly smaller (more than a factor of 10) than the suspended transport for current velocities larger than about 1 m/s; the bed-load transport approaches the suspended transport of sand in the range of 400–600 μm for small velocities close to initiation of motion. Fig. 5 shows that the effect of sand diameter (between 60 and 600 μm) on suspended sand transport is largest at low velocities, but gradually reduces for larger velocities (larger than about 1.4 m/s).

Coastal Flow Conditions

Field data sets for combined current and wave conditions in the coastal zone are rather scarce. Herein, some field data sets of Egmond beach along the coast of The Netherlands are used

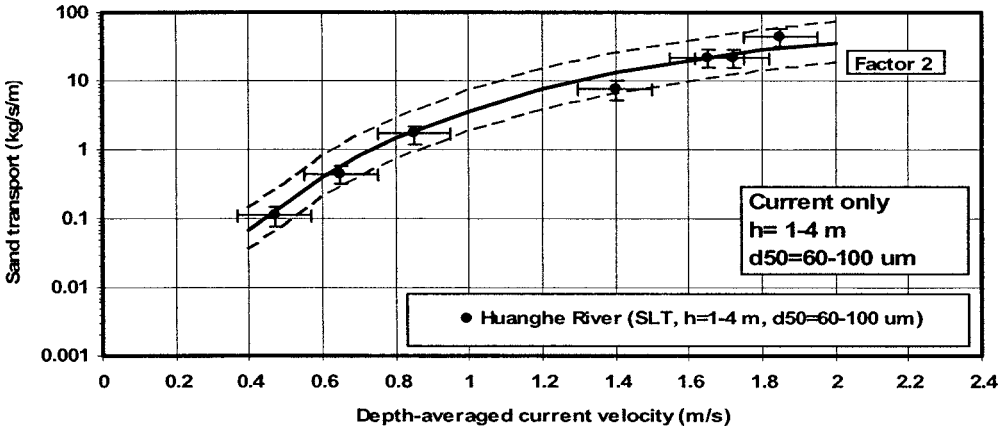

Fig. 1. Suspended transport as function of current velocity for d_{50}=60–100 μm; river flow

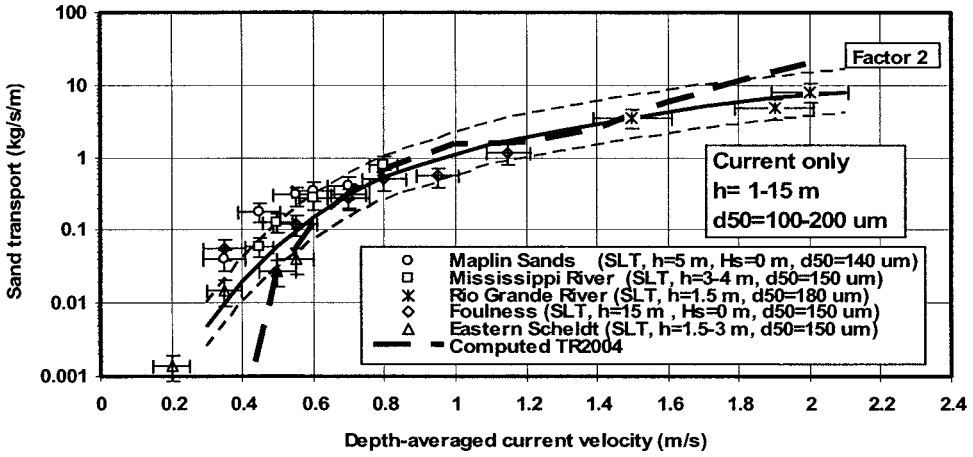

Fig. 2. Suspended transport as function of current velocity for d_{50}=100–200 μm; river and tidal flow

(Kroon 1994; Wolf 1997; Grasmeijer 2002; van Rijn et al. 2001). Fig. 6 shows the suspended sand transport rates (including variation ranges) as a function of depth-averaged velocity for depths between 1 and 2 m and sand in the range of 200–400 μm. The trend line for conditions with current only (H_s=0 m; see Fig. 3) is shown for comparison. The sand transport in the coastal zone is found to be strongly dependent on the relative wave height (H_s/h), particularly for small velocities (0.1–0.6 m/s). The transport of sand in the size range 200–400 μm increases by a factor of 10–100 when waves with a relative wave height of about 0.4–0.5 are superimposed on a current of about 0.1–0.6 m/s. Thus, the waves are very effective in the stirring of sand from the bed into the water column. The trend seems to indicate that the increase of the transport due to the wave effect decreases with increasing current velocity.

Modeling of Suspended-Load Transport

Vertical Distribution of Concentrations

Observations of the vertical distribution of the sediment concentration show the presence of large concentrations near the bed, which gradually decrease towards the water surface, depending on the effective fall velocity, the bed-shear velocity (as a measure of diffusivity) and the near-bed Richardson number (as a measure of turbulence damping). This system can be represented by the time-averaged (over the wave period) advection–diffusion equation

$$cw_s + \varepsilon_{s,cw} dc/dz = 0 \tag{2}$$

where w_s=fall velocity of suspended sediment in a fluid–sediment mixture (m/s), $\varepsilon_{s,cw}$=sediment mixing coefficient for combined steady and oscillatory flow (m^2/s), c=time-averaged volume concentration at height z above the bed. Flocculation, hindered settling, and turbulence damping effects are taken into account. Eq. (2) has been shown to work well for steady flow (Vanoni 1977). Based on experimental data, van Rijn (1993) has shown that Eq. (2) can also be used to compute the time-averaged concentrations in oscillatory flow, provided that an effective diffusivity related to basic wave parameters is used. Coleman (1970) has shown that the sediment diffusivity in steady flow is larger (up to a factor of 5 at middepth) than the fluid momentum diffusivity and increases for increasing values of w_s/u_*. Sistermans (2002) has reanalyzed the Enoree River data used by Coleman (1970) and shows that the diffusivity is almost constant for most data or only very weakly increasing with increasing w_s/u_* for some cases. Sistermans (2002) thinks that Coleman (1970) has systematically underestimated the settling velocities of the finer

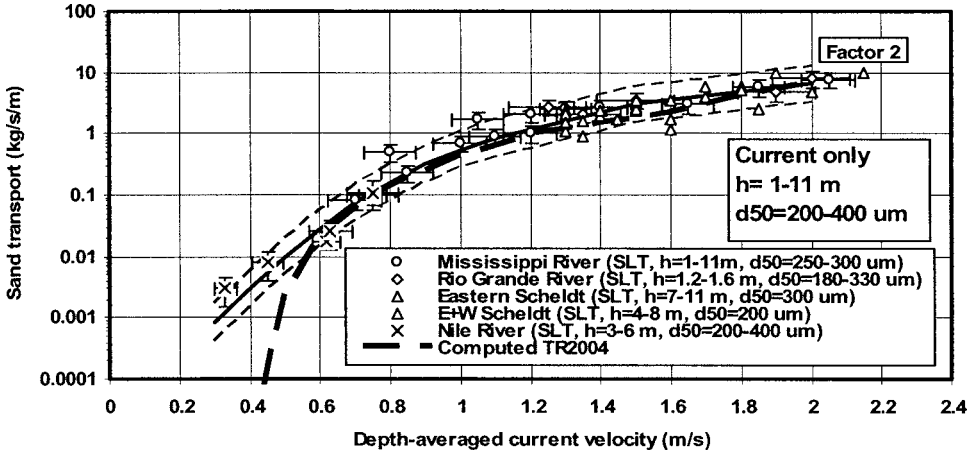

Fig. 3. Suspended transport as function of current velocity for d_{50}=200–400 μm; river and tidal flow

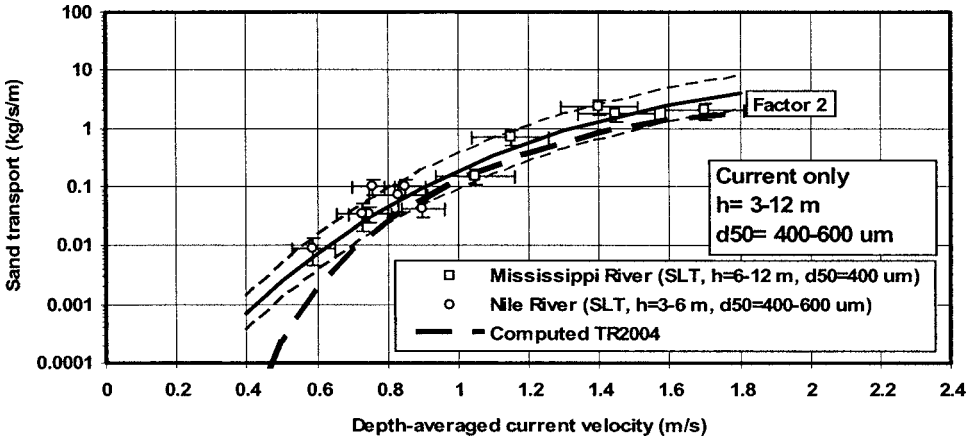

Fig. 4. Suspended transport as function of current velocity for d_{50}=400–600 μm; river and tidal flow

sediment fractions. Based on analysis of measured concentration profiles with sediment fraction sizes in the range of 50–600 μm,Sistermans (2002) concludes that the time-averaged concentrations in steady and oscillatory flow can be computed by the gradient diffusion model and that the sediment diffusivity is not dependent on particle size. Nielsen and Teakle (2004) show that the sediment diffusivity can be larger or smaller than the fluid diffusivity depending on the relative magnitude of the vertical decay length scales of the velocity and concentration profiles. Nielsen (1992) is of the opinion that pure gradient diffusion is inadequate as a model for suspended sediments, if the sediment diffusivity is different for different particle sizes. He proposes a convection–diffusion-type approach, which can better deal with vortex trapping effects for sediments in oscillatory flow.

Sediment Mixing Coefficient

For combined steady and oscillatory flow the sediment mixing coefficient (see Fig. 7) is modeled as

$$\varepsilon_{s,cw} = [(\varepsilon_{s,c})^2 + (\varepsilon_{s,w})^2]^{0.5} \tag{3a}$$

where $\varepsilon_{s,w}$=wave-related mixing coefficient (m^2/s); $\varepsilon_{s,c}$ $=\phi_d\beta_c\varepsilon_{f,c}$=current-related mixing coefficient due to main current (m^2/s) (van Rijn 1984a,b,c, 1993); the effect of the sediment particles on the mixing of fluid momentum is taken into account by the β_c factor, which depends on the particle fall velocity of the suspended sand particles and the bed-shear velocity; and $\beta_c=1+2(w_s/u_{*,c})^2$ with $\beta_c \leq 1.5$. The damping of turbulence due to the presence of high sediment concentrations in the near-bed layer is taken into account by the ϕ_d parameter. Similarly, $\varepsilon_{s,w}=\phi_d\beta_w\varepsilon_{f,w}$. Some parameters of the wave-related sediment mixing coefficient have recently been modified (van Rijn 1993, 2000). The vertical distribution has not been changed (Fig. 7). The thickness of the sediment mixing layer near the bed reads as

$$\delta_s = 2\gamma_{br}\delta_w, \quad \text{with limits } 0.1 \leq \delta_s \leq 0.5 \text{ m} \tag{3b}$$

where δ_s=thickness of effective near-bed sediment mixing layer; δ_w=thickness of wave boundary layer=$0.36A_\delta(A_\delta/k_{s,w,r})^{-0.25}$; A_δ=peak orbital excursion based on significant wave height H_s (m); $k_{s,w,r}$=wave-related bed roughness; and $\gamma_{br}=1+(H_s/h-0.4)^{0.5}$=empirical coefficient related to wave breaking ($\gamma_{br}=1$ for $H_s/h \leq 0.4$).

The wave-related sediment mixing coefficient in the upper half of the water column has been modified into

$$\varepsilon_{s,w,\max} = 0.035\gamma_{br}hH_s/T_p \quad \text{with } \varepsilon_{s,w,\max} \leq 0.05 \text{ m}^2/\text{s} \tag{4a}$$

The wave-related sediment mixing coefficient near the bed is described by

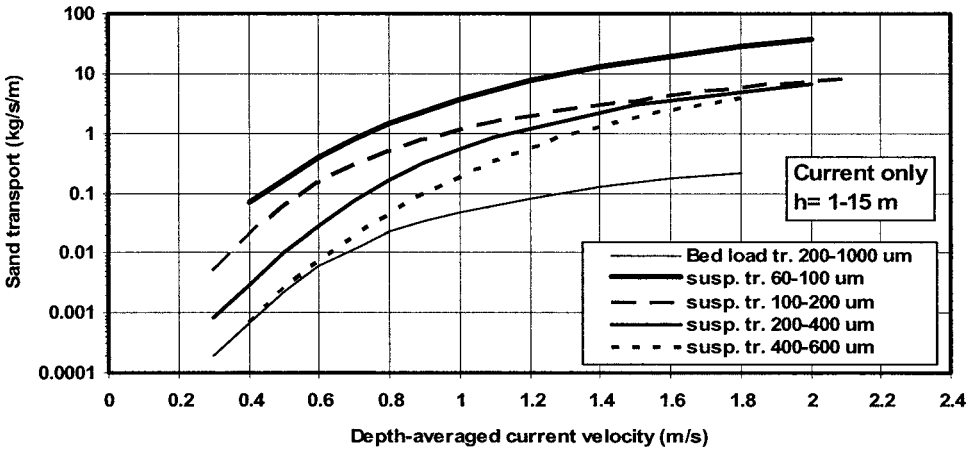

Fig. 5. Trend lines of bed-load transport and suspended transport as function of current velocity and particle size; river and tidal flow

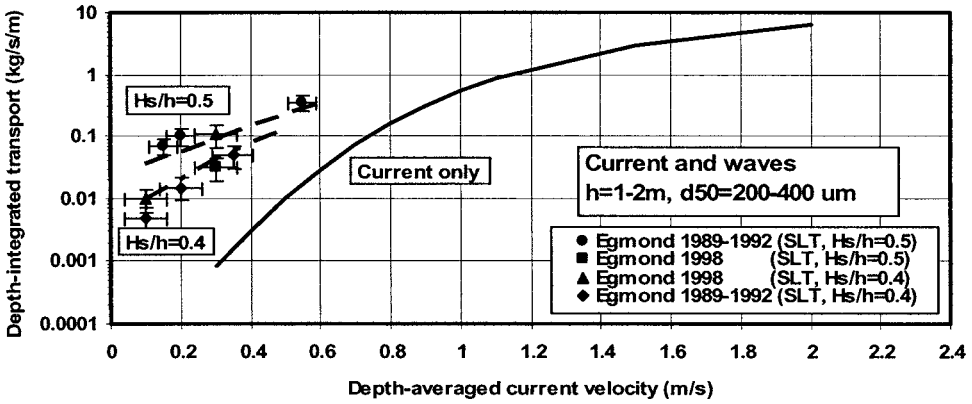

Fig. 6. Suspended transport as function of current velocity; coastal flow

$$\varepsilon_{s,w,\text{bed}} = 0.018\gamma_{\text{br}}\beta_w\delta_s U_{\delta,r} \tag{4b}$$

where $U_{\delta,r}$=representative near-bed peak orbital velocity based on significant wave height; δ_s=thickness of mixing layer; β_w=coefficient=$1+2(w_s/u_{*,w})^2$ with $\beta_w \leq 1.5$; w_s=fall velocity of suspended sand; and $u_{*,w}$=wave-related bed-shear velocity.

The effect of breaking waves is taken into account by an empirical enhancement factor (γ_{br}) related to relative wave height and acting on the effective mixing coefficient [see Eqs. (4*a*) and (4*b*)]. This approach works well for breaking waves in the surf zone (Grasmeijer and van Rijn 2001).

The near-bed mixing parameter $\varepsilon_{s,w,\text{bed}}$ was found to be slightly dependent on the particle size, based on analysis of sand concentration profiles of experiments with bed material in the range of 100–300 μm (van Rijn 1993). The near-bed mixing appears to increase slightly with increasing particle size, which may be an indication of the dominant influence of centrifugal forces acting on the particles due to strong vortex motions in rippled bed conditions (vortices are not small compared to the vertical decay scale of the concentration profile; see Nielsen 1991, Nielsen and Teakle 2004), resulting in an increase of the effective mixing of sediment particles. This effect, which is stronger for coarser particles, is modeled by the β factor. Given the controversy about the sediment diffusivity and the fact that not much information is available for bed materials larger than about 300 μm, the application of the β factor is highly uncertain for coarse sediments or very small bed-shear velocities. Therefore, herein the maximum value of β is set to 1.5.

For steady river flow the parabolic sediment diffusivity (over the full depth) yields the well-known Rouse profile: $c/c_a=\{[(h-z)/z][a/(h-a)]\}^{w_s/\kappa u_*}$; with h=water depth; a=reference level; z=height above bed; c_a=reference concentration; w_s=particle fall velocity; u_*=bed-shear velocity; and κ=von Kármán coefficient (=0.4). The relative importance of the suspended load transport is determined by the suspension number $Z=w_s/\kappa u_*$. The following ranges are given: $Z=5$: suspended sediment in near-bed layer ($z<0.1h$); $Z=2$: suspended sediment up to mid of water depth ($z<0.5h$); $Z=1$: suspended sediment up to water surface ($z<h$); and $Z=0.1$: suspended sediment almost uniformly distributed over water depth. In the case of relatively coarse sediments (>100 μm; $Z>1$) the middepth concentration generally is much smaller than the near-bed concentration ($c_{\text{mid}}/c_{\text{bed}} \ll 1$). For finer sediments this ratio gradually approaches unity ($Z<1$).

Near-Bed Concentration

For modeling purposes it is essential to know the behavior of the near-bed concentration as a function of the flow regime and the

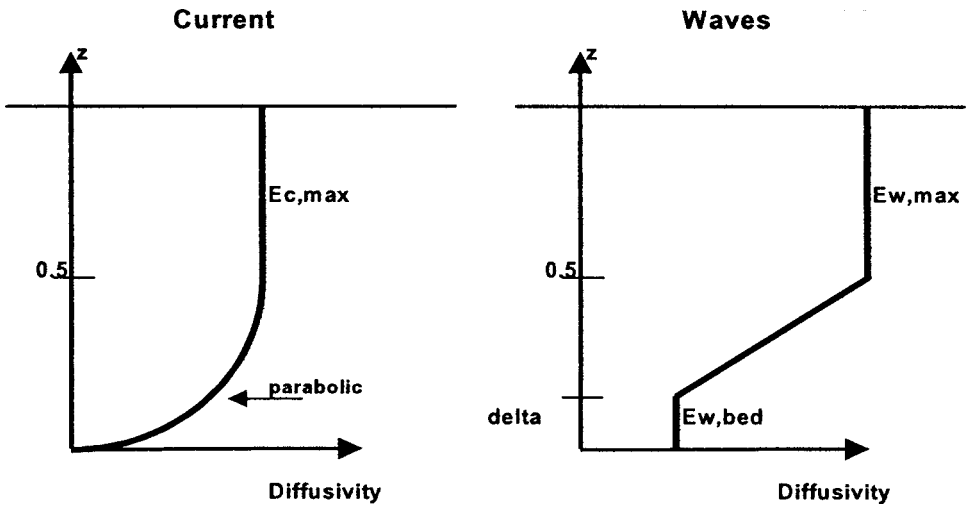

Fig. 7. Vertical distribution of mixing coefficients

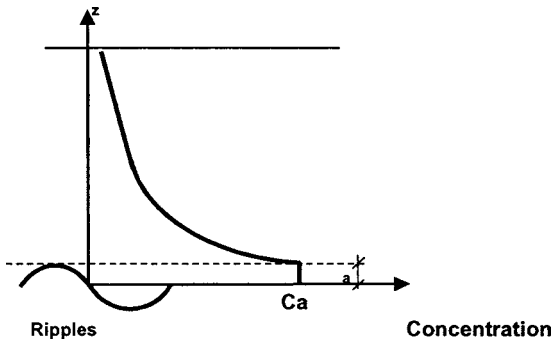

Fig. 8. Reference concentration

particle size. The reference volume concentration (see Fig. 8) close to the bed is given by (van Rijn 1984a,b,c, 1993)

$$c_a = 0.015(1 - p_{\text{clay}}) f_{\text{silt}} \frac{d_{50}}{a} \frac{T^{1.5}}{D_*^{0.3}}$$

$$\text{with } c_a \leq 0.05 \text{ (maximum value of about 150 kg/m}^3\text{)} \tag{5}$$

where $D_* = d_{50}[(s-1)g/\nu^2]^{1/3}$=dimensionless particle parameter; T=dimensionless bed-shear stress parameter; d_{50}=median particle size of bed material, $f_{\text{silt}} = d_{\text{sand}}/d_{50}$=silt factor ($f_{\text{silt}}=1$ for $d_{50} > d_{\text{sand}}=62$ μm); and a=reference level (m), where a is defined as the maximum value of half the wave-related and half the current-related bed roughness values. Thus, $a=\max(0.5k_{s,c,r}, 0.5k_{s,w,r})$ with a minimum value of 0.01 m. In the case of sheet flow conditions in the upper transport regime the reference level is related to the sheet flow layer roughness [set to $20d_{50}$] with a minimum value of 0.01 m. Bed roughness expressions are specified in other paper.

Eq. (5) specifies the sediment concentration at a small height above the bed (or fluid mud bed).

The T parameter is

$$T = (\tau'_{b,cw} - \tau_{b,\text{cr}})/\tau_{b,\text{cr}} \tag{6}$$

where $\tau'_{b,cw}$=time-averaged effective bed-shear stress (N/m^2); and $\tau_{b,\text{cr}}$=time-averaged critical bed-shear stress according to Shields (N/m^2).

The magnitude of the time-averaged bed-shear stress, which is independent of the angle between the wave- and current direction, is given by (in line with Bijker 1971)

$$\tau'_{b,cw} = \tau'_{b,c} + \tau'_{b,w} \tag{7}$$

where $\tau'_{b,c} = \mu_c \alpha_{cw} \tau_{b,c}$=effective current-related bed-shear stress (N/m^2), and $\tau'_{b,w} = \mu_w \tau_{b,w}$=effective wave-related bed-shear stress (N/m^2); μ_w=wave-related efficiency factor; and α_{cw}=wave–current interaction factor (van Rijn 1993).

The current-related efficiency factor is defined as

$$\mu_c = f'_c/f_c \tag{8}$$

with: f'_c=grain-related friction coefficient based on $1d_{90}$; and f_c=current-related friction coefficient based on predicted bed roughness values.

The wave-related efficiency factor μ_w is an important parameter, because it strongly affects the reference concentration near the bed in combined wave–current conditions. This parameter will probably depend on the bed material and bed form characteristics, but the functional relationship involved is not yet known. In particular, vortex motions around ripples are very effective in the stirring of sediment from the bed. Based on a very limited dataset (van Rijn 1993), the μ_w factor was found to be related to particle size D_*. Since 1993 much more reliable data sets have become available, therefore the μ_w factor has been recalibrated to get the best possible estimate of the near-bed concentration (see below), yielding

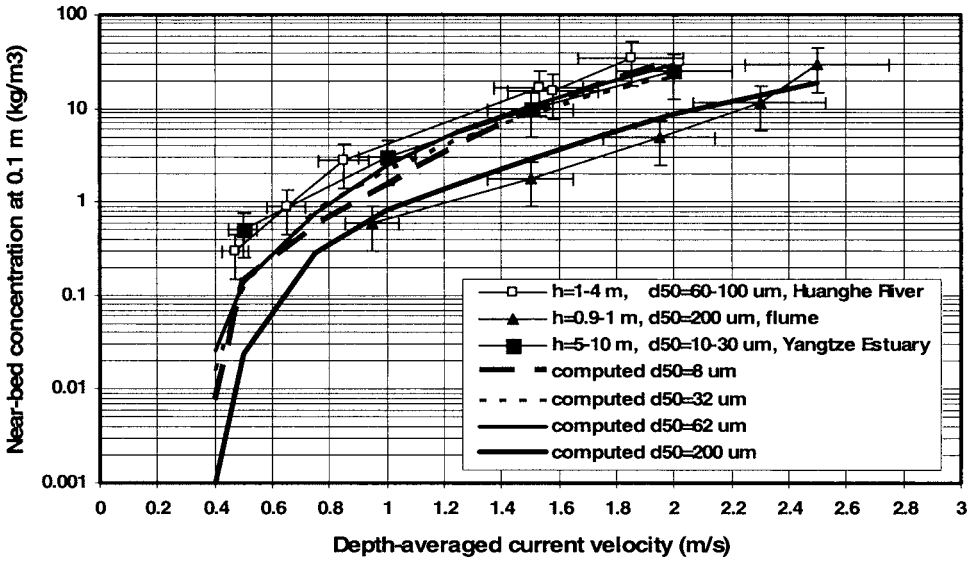

Fig. 9. Measured and computed near-bed concentrations (at about 0.1 m above bed) as function of depth-averaged current velocity and particle size (8–200 μm)

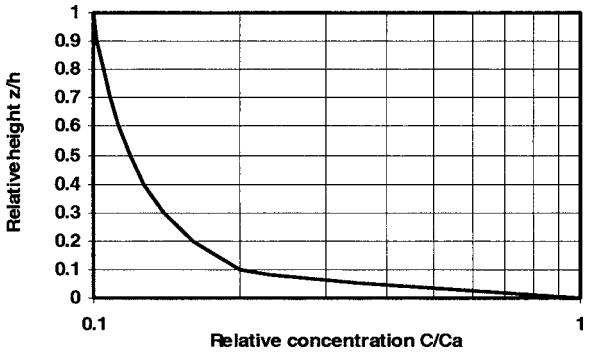

Fig. 10. Typical sediment concentration profile with flocculated suspended sediments above mud bed in Changjiang Estuary, China

$$\mu_w = 0.7/D_* \quad \text{with} \quad \mu_{w,\min} = 0.14 \quad \text{for} \quad D_* \geq 5$$
$$\text{and} \quad \mu_{w,\max} = 0.35 \quad \text{for} \quad D_* \leq 5 \tag{9}$$

It is noted that Eq. (9) is only slightly different from that found by van Rijn (1993). Eq. (5) predicts the sediment concentration at the top of the bed load layer, which is assumed to be equal to half the ripple roughness height in the lower regime (see Fig. 8) or the thickness of the sheet flow layer (of the order of 0.01 m) in the upper regime. Eq. (5) was derived for natural sediment beds with particle sizes larger than about 100 μm, but it also yields quite realistic values for fine sediment beds in the range of 60–100 μm as observed in the Huanghe River in China (see below). The basic parameters influencing the near-bed concentrations in the silt range of 8–62 μm are not very well known. The limited data available seem to suggest that the near-bed concentrations of particles in the silt range (8–62 μm) are approximately constant; independent of grain size (see Fig. 9). The T parameter [Eq. (6)] is approximately constant for a given bed-shear stress, because the critical bed-shear stress is approximately constant in the silt range. Hence, a constant near-bed concentration can be obtained by introducing a silt factor [$f_{\text{silt}}=d_{\text{sand}}/d_{50}$, see Eq. (5)]. This latter approach will herein tentatively be used for the silt range (<62 μm). It is noted that in the silt range it may be more realistic to apply an entrainment function. Assuming local equilibrium, this function can be derived from $E=w_s c_a$ (van Rijn 1987), resulting in a sediment entrainment function related to bed-shear stress and sediment characteristics.

Fig. 9 shows measured near-bed concentrations at about 0.1 m above the bed as a function of depth-averaged flow velocity. The data are taken from a large-scale flume experiment (Delft Hydraulics 1985; Voogt et al. 1991) and from the Huanghe River (Van den Berg and Van Gelder 1993) and Yangtze Estuary (Li 1991; Li et al. 1993, 2000, 2004) in China. The near-bed concentration varies in the range of 0.5–50 kg/m^3 for increasing velocities up to 2.5 m/s. The near-bed concentrations of 200 μm sediment are much smaller (factor of 5) than those of fine silts in the range of 5–100 μm. The near-bed concentrations do not seem to be much affected by particle size for fine sediments in the silt range (<62 μm), as the near-bed concentrations of the Huanghe River (60–100 μm bed) and the Yangtze Estuary (10–30 μm bed) are of the same order of magnitude. Computed near-bed concentrations at $z=0.1$ m for a water depth of 10 m and particle size in the range of 8–200 μm [$T=15°$C and salinity (Sa)=30 parts per thousand (ppt)] are also shown in Fig. 9. The computed values based on Eq. (5) are in reasonably good agreement for 200 μm sediment (water depth of 10 m, $T=15°$C and Sa=30 ppt), but are somewhat too small (factor of 2–3) for silts in the range of 8–62 μm. Neglecting the silt factor, the predicted near-bed concentrations will be considerably smaller (factor of 8 for sediment of 8 μm). Additional field data sets in the silt range are necessary to determine better the precise value of the silt factor. It may also be necessary to use a constant particle size in the silt range as very fine sediments will be eroded as chunks/aggregates or flocs rather than as single particles (Roberts et al. 1998). The presence of organic materials and biological effects may considerably reduce the near-bed concentration.

Suspended Sediment Size, Fall Velocity, and Flocculation

As completely uniform beds do not exist, the suspended sediments (d_s) generally are somewhat smaller ($d_s=0.5$–$1d_{50,\text{bed}}$) than that of the bed depending on the composition (grading) of the bed and the strength of the flow and wave motion. Based on analysis of experimental data, the suspended sediment size is estimated by

$$\begin{aligned} d_s &= [1 + 0.0006(d_{50}/d_{10} - 1)(\psi - 550)]d_{50} && \text{for } \psi < 550 \text{ and } d_{50} > d_{\text{silt}} \\ d_s &= d_{50} && \text{for } \psi \geq 550 \text{ and } d_{50} > d_{\text{silt}} \\ d_s &= d_{50} && \text{for } d_{50} < d_{\text{silt}} \\ d_s &= 0.5 d_{\text{silt}} && \text{for } d_{50} < 0.5 d_{\text{silt}} \end{aligned} \tag{10}$$

where ψ=mobility parameter=$U_{wc}^2/[(s-1)gd_{50}]$ with $(U_{wc})^2=(U_w)^2+u_c^2$; U_w=peak orbital velocity near bed, $s=\rho_s/\rho_w$=relative density; and u_c=depth-averaged current velocity. The lower limit is set to $d_{s,\min}=0.5(d_{10}+d_{50})$. Eq. (10) yields realistic results for weakly graded sediment beds smaller than about 1,000 μm (see Figs. 1–4), but overpredicts for very graded beds. In the latter case the multifraction method should be used. In the sand range (>62 μm) the d_s value decreases with increasing grading (d_{50}/d_{10}) of the bed and with decreasing flow strength (ψ). In the fine silt range (8–32 μm), it is not realistic to assume that the suspended material solely consists of single particles; flocculation effects are often observed to play a major role, particularly in tidal flow with saline water. The vertical distribution of fine sediment concentrations over a tidal flat of about 10 μm in the Changjiang Estuary (mouth of the Yangtze River) in China was studied by Li (1991) and Li et al. (2000), yielding $c_{\text{mid}}/c_{\text{bed}}$ ratios in the range of 0.1–0.5 in water depths of 1–3 m and velocities of 0.3–1 m/s. Using these values, the effective fall diam-

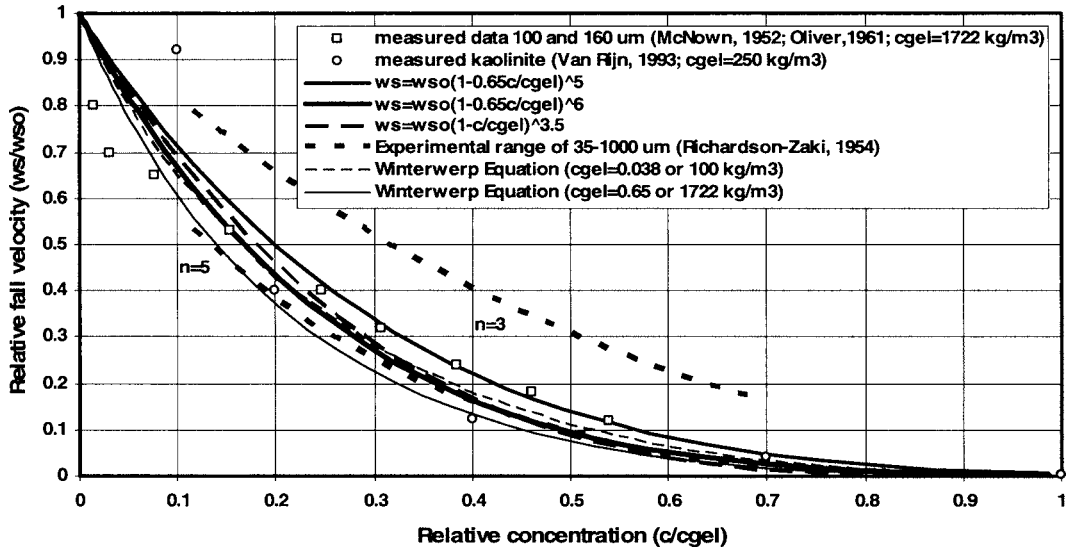

Fig. 11. Hindered settling effect; relative fall velocity as function of relative concentration

eter (based on a density of 2,650 kg/m^3) is estimated to be about 30–40 μm, which is much larger than the bed material of 10 μm indicating the presence of flocculation effects. Shi and Zhou (2004) also studied the effective settling velocity of fine flocculated sediments above mud beds in the Changjiang Estuary in China. Most of the sediments in this estuary are smaller than 32 μm. Acousting profiling instruments and point water samples were used to measure the sediment concentration profiles in a depth of 6–10 m. A typical concentration profile is shown in Fig. 10. The concentration decreases by a factor of about 5 in the near-bed layer ($z<0.1$h) and by a factor of 2 to 3 in the upper layer between 0.1h and h, which can only be explained by flocculated settling processes. Based on fitting of Rouse-type concentration profiles, the effective settling velocity was found to vary with the sediment concentration as follows: $w_s=0.6$ mm/s for $c=0.2$ kg/m^3, $w_s=1$ mm/s for $c=0.5$ kg/m^3 and $w_s=2$ mm/s for $c=1$ kg/m^3 (Shi and Zhou 2004). The increase of the settling velocity with concentration is a clear indication of flocculation effects. Similar results have been found by Vinzon and Mehta (2003) at the mouth of the Amazon in Brazil and by Thorn (1981) for the Severn Estuary in the United Kingdom.

Herein, it is assumed that the effective suspended sediment diameter increases with concentration due to the flocculation effect with a minimum value of 16 μm. Using this approach, it is demonstrated that the ratio $c_{\text{mid}}/c_{\text{bed}}$ is of the order of 0.1–0.5 as observed for fine sediment beds. In situ floc measurements show that the actual floc sizes in the water column are much larger (up to the order of 1 mm), but these flocs have a much lower density (1,100–1,200 kg/m^3). However, the effective fall velocity is about the same (of the order of 1–2 mm/s). Using these values during slack tide (of about 2 h) without much flow, almost full deposition of the suspended load in a water depth of about 10 m can take place resulting in a fluid mud bed.

The sediment fall velocity is given by

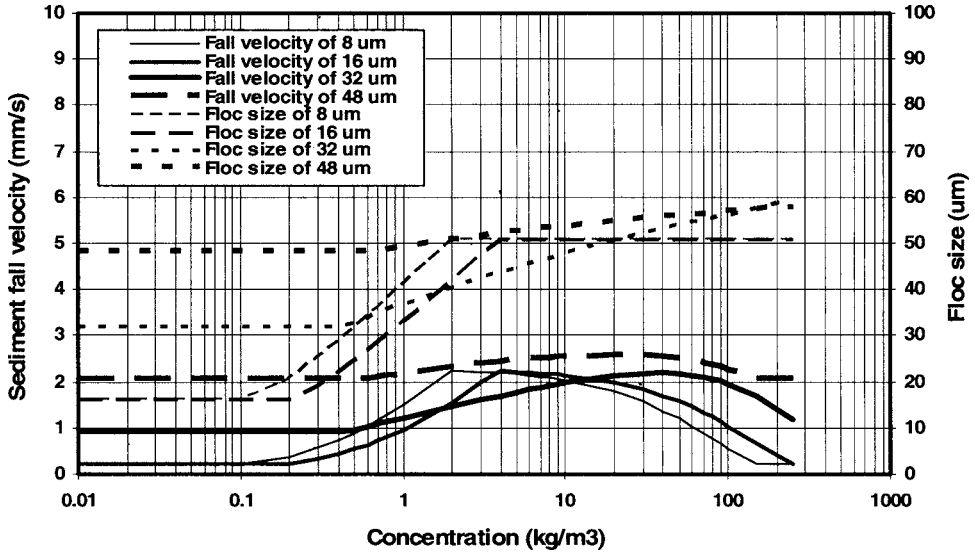

Fig. 12. Effective fall velocity and floc size as a function of concentration for a bed of 8, 16, 32, and 48 μm

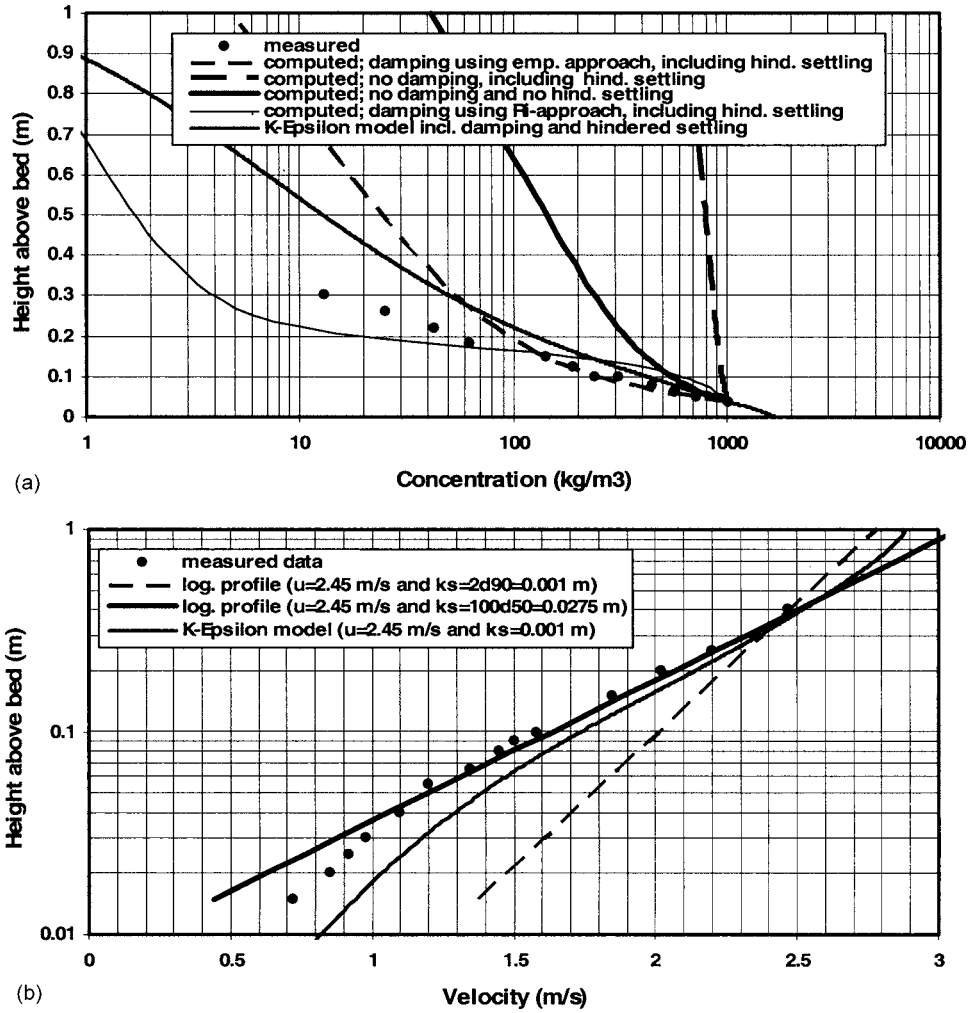

Fig. 13. Effect of hindered settling and turbulence damping on concentration profile (a) and velocity profile (b), Run S-15 (adapted from Einstein and Chien 1955) (see cases in Table 2)

$$w_s = \phi_{floc}\phi_{hs}w_{s,o} \tag{11}$$

with: ϕ_{floc}=flocculation factor; ϕ_{hs}=hindered settling factor; and $w_{s,o}$=sediment fall velocity of single suspended particles in clear water (van Rijn 1984a,b,c, 1993) based on suspended size from Eq. (10). The minimum fall velocity is set to 0.2 mm/s assuming a minimum floc size of about 16 μm. Based on the experimental data of Thorn (1981), Shi and Zhou (2004), and Vinzon and Mehta (2003), the flocculation factor (for particles finer than d_{sand} and Sa≥5 ppt) is herein proposed to be represented by

$$\phi_{floc} = [4+^{10}\log(2c/c_{gel})]^{\alpha}$$

with minimum value of 1 and maximum value of 10 (12)

where $\alpha=(d_{sand}/d_{50})-1$ with $\alpha_{min}=0$ and $\alpha_{max}=3$; c=mass concentration ($=\rho_s c_{volume}$); and c_{gel}=gelling mass concentration (between 130 and 1722 kg/m^3). The α factor varies linearly between 0 and 3 depending on the ratio of d_{sand} and d_{50}; $\alpha=0$ for $d_{50}=62$ μm (sand, $\phi_{floc}=1$) and $\alpha=3$ for $d_{50}\leq 16$ μm. The ϕ_{floc}-factor varies in the range of 1–10 for concentrations varying between 0.1 and 10 kg/m^3, as observed by Shi and Zhou (2004) and Vinzon and Mehta (2003). The ϕ_{floc} factor gradually increases for particles decreasing from 62 to 16 μm. Flocculation is supposed to be fully active for a salinity value larger than about 5 ppt. Assuming that the effective fall velocity is proportional to d^2 for fine sediment, it follows that the effective floc size (based on density of 2,650 kg/m^3) is given by

$$d_{floc} = (\phi_{floc})^{0.5\alpha}d_s \quad \text{with } d_{floc,min} = 16\ \mu\text{m (minimum floc size)} \tag{13}$$

Hindered Settling

In high-concentration flows the suspended sediment particles cannot settle freely, because of the presence of the surrounding particles. This process is known as hindered settling and consists of various effects: flow and wake formation around the particles and the increase of density and viscosity of the suspension. Hindered settling effect was studied experimentally by Richardson and Zaki (1954) and Richardson and Meikle (1961) using glass-type particles (ballotini) with particle sizes in the range of 35–1,000 μm and alumina powder with a particle size of about 5 μm. They found that the hindered settling effects can be represented as: $w_s=w_{s,o}(1-c)^n$ with c=volume concentration and $w_{s,o}$=settling velocity in clear water. The n coefficient varies almost linearly from $n=5$ for $R=w_{s,o}d/v<1$ to $n=3$ for $R=100$. The n coefficient of the very fine alumina powder was about 10 indicating a very strong decrease of the settling velocity with increasing con-

centration. Fig. 11 shows their results for glass particles in the range of 35–1,000 μm (Reynolds numbers $w_{s,o}d/v$ between 1 and 100) and the results of McNown and Lin (1952) and Oliver (1961). The results are plotted using a relative concentration c/c_{gel} with $c_{gel}=0.65$ (volume) or 1,722 kg/m^3 for noncohesive material. Experimental results for very fine clay material (kaolinite) are also shown. These values are based on tests in a small settling column with kaolinite of 5–10 μm and a maximum settling velocity of 0.09 mm/s (in saline water; van Rijn 1993) and $c_{gel}=250$ kg/m^3.

The hindered settling (hs) factor is herein represented by the Richardson–Zaki expression (Richardson and Zaki 1954), which is formulated in terms of the volume concentration as

$$\phi_{hs} = w_s/w_{s,o} = (1-c)^5 \quad (14a)$$

$$\phi_{hs} = (1-0.65c/c_{gel})^5 \quad (14b)$$

where c=volume concentration (including wash load); and c_{gel}=volume concentration of immobile sediment bed. Eqs. (14*a*) and (14*b*) are similar for $c_{gel}=0.65$ (pure sand). Eq. (14*b*) is presented in Fig. 11. Eq. (14*b*) yields the best results for fine sand with volume concentrations in the range of 0.1–0.35. The exponent needs to be somewhat larger to better represent the hindered settling of clay material. The experimental hindered settling results for fine sediments (8–200 μm) can be represented by a simple power relationship $w_s=w_{s,o}(1-0.65c/c_{gel})^n$ with an exponent n in the range of 5–6. Another expression $\phi_{hs}=(1-c/c_{gel})^{3.5}$ can also be used to describe the experimental results of fine sediments (Fig. 11). Winterwerp (1999) has proposed a new expression that is generally valid

$$\phi_{hs} = w_s/w_{s,o} = (1-c/c_{gel})^2(1-c)/(1+2.5c/c_{gel}) \quad (14c)$$

Eq. (14*c*), shown in Fig. 11 for two extreme c_{gel} values, is in good agreement with measured values for the sand range but underpredicts slightly for the mud range.

Herein, Eq. (14*b*) has been used. The effect of the concentration on the fluid viscosity is herein neglected as it is assumed that this effect is implicitly represented by the empirical hindered settling function. The effective sediment fall velocity including flocculation and hindered settling effects based on Eqs. (11)–(14) is shown in Fig. 12 for particle sizes of $d_{50}=8$, 16, 32, and 48 μm (kinematic viscosity coefficient=1×10^{-6} m^2/s). The effective fall velocity of mud bed particles of 8 μm increases from 0.2 mm/s for $c=0.1$ kg/m^3 to 2 mm/s for $c=2$ kg/m^3, as observed by Shi and Zhou (2004). The flocculation process of a mud bed of 16 μm particles proceeds somewhat slower. Hindered settling effects are dominant for $c>5$ kg/m^3. The effective floc size of mud bed particles of 16 μm varies between 16 and 50 μm. The effective fall velocity of 32 μm bed increases from about 0.9 mm/s for $c=0.1$ kg/m^3 to 2.2 mm/s for $c=30$ kg/m^3. Hindered settling effects dominate for $c>30$ kg/m^3. The effective floc size of mud bed particles of 32 μm varies between 32 and 60 μm. Flocculation for particles of 48 μm mud bed is of minor importance (see Fig. 12). When wash load is present, the fall velocity of the sand fraction is affected by the wash load through the hindered settling effect. The hindered settling effect should then be based on the total sediment concentration (sand+wash load concentration).

Stratification Effects

Stratification effects due to the presence of sediment particles are important in the upper regime with high sediment concentrations.

Table 2. Modeling Approaches Related to Stratification Effects of Run S-15 [Adapted from Einstein and Chien (1955)]

Case	Depth-integrated sand transport (kg/s/m)
Measured data Run S-15	14
No hindered settling and no damping	50
Velocity according to logarithmic profile (k_s=1 mm)	
Concentration according to Rouse-type profile (k_s=1 mm)	
No damping	260
Velocity according to logarithmic profile (k_s=1 mm)	
Concentration according to diffusion equation with hindered settling (k_s=1 mm)	
Damping based on Richardson number [$\varepsilon_s=\phi_d\varepsilon_f$ with $\phi_d=(1+15R^{0.5})^{-1}$]	19
Velocity according to logarithmic profile ($k_{s,a}=100d_{50}$=27.5 mm)	
Concentration according to diffusion equation with hindered settling (k_s=1 mm)	
Damping based on empirical function [$\varepsilon_s=\phi_d\varepsilon_f$ with $\phi_d=1+f(c)$][a]	15
Velocity according to logarithmic profile ($k_{s,a}=100d_{50}$=27.5 mm)	
Concentration according to diffusion equation with hindered settling (k_s=1 mm)	
Damping based on k-epsilon model ($C_{3\varepsilon}=-1.4$)[b]	18
Velocity based on eddy viscosity (k_s=1 mm)	
Concentration based on eddy viscosity (k_s=1 mm)	

[a]van Rijn (1984a,b,c).

[b]Burchard and Baumert (1995).

Most of the experimental evidence (Winterwerp 2001) suggests that the sediment particles have a damping effect on the turbulence parameters (eddy viscosity/diffusivity), and hence, on the velocity profile and the sediment concentration profile resulting in lower near-bed velocities and concentrations. Herein, the damping of turbulence due to the presence of high sediment concentrations in the near-bed (sheet flow) layer is taken into account by a damping coefficient ϕ_d ($=\varepsilon_s/\varepsilon_f$ with ε_s=sediment diffusivity and ε_f=fluid diffusivity).

Stratification effects can be clearly demonstrated by analyzing one of the classical experiments of Einstein and Chien (1955). Fig. 13 shows the measured velocity and concentration profiles of their Run S-15 (h=depth=0.124 m, u=2.45 m/s, S=water surface slope=0.0168, d_{50}=275 μm, and T=18°C). This test is related to high-concentration flow of water and sand (near-bed concentration of about 1,025 kg/m^3 and about 10 kg/m^3 at 0.3 h; d_{50}=270 μm, $d_{10}\cong$200 μm, and $d_{90}\cong$500 μm) over a rigid bed (of the same material) with water depth of h=0.124 m, depth-averaged velocity of u=2.45 m/s in middle of flume. The bed roughness derived from the water surface slope is about k_s=1 mm (about $2d_{90}$). The sediment transport over the rigid bed is about 14 kg/s/m. Various modeling approaches are herein explored to determine the relative importance of the stratification effects; see Table 2. Fig. 13 shows the computed concentration and velocity profiles of Run S-15 of Einstein and Chien (1955). The measured near-bed concentration c_a=1,025 kg/m^3 at z=0.005 m was used as bed boundary condition.

Table 3. Sediment Transport Data near Li-Jin of Huanghe River in China (September 1987)

Case	Water depth h (m)	Depth-averaged flow velocity u (m/s)	Sediment size d_{50} (μm)	Sediment size d_{90} (μm)	$q_{s,\text{measured}}$ <32 μm (kg/s/m)	$q_{s,\text{measured}}$ >32 μm (kg/s/m)	Modified $q_{s,\text{computed}}$ >32 μm (kg/s/m)	Original $q_{s,\text{computed}}$ >32 μm (kg/s/m)
1+2	3.5	1.85±0.1	80	105	115	44±12	61.3	74.2
3+8	1.72	1.58±0.1	87	115	35	22±10	20.2	22.0
4+9	1.15	1.4±0.1	85	105	20	7.5±1	9.8	10.9
5+6+7	3.65	1.65±0.05	63	90	50	22±8	45.5	68.4
10	2.7	0.85	74	99	7	1.7	0.96	1.43
11	2.2	0.65	64	90	4	0.45	0.36	0.63
12	1.1	0.47	60	85	2	0.11	0.056	0.10

Neglecting hindered settling and the damping of turbulence (reduction of eddy viscosity), the velocities can be described by a logarithmic profile and the sediment concentrations by a Rouse-type profile (using measured value in lowest point as reference concentration), resulting in a transport rate of about 50 kg/s/m (factor of 4 larger than the measured value). As can be observed in Fig. 13, the computed velocities and concentrations are much too large in the near-bed zone. The overprediction due to errors in the velocity profile can be easily represented by using an apparent bed roughness of about $k_{s,a}=100d_{50}=0.0275$ m. This latter value can be seen as a measure of the vertical scale of the sheet flow layer thickness. Using this value, the velocity profile can be very well represented (Fig. 13). It should be realized that this apparent roughness is not the physical roughness (shear) affecting the turbulent mixing processes. The bed roughness derived from the surface slope is not larger than about 1 mm, because the mixing processes are damped resulting in reduced shear and roughness (hence, mixing based on $k_s=1$ mm).

Taking only hindered settling into account but neglecting the damping effects, the computed concentrations are almost uniform over the depth (see Fig. 13) due to the strong reduction of the settling velocities resulting in a transport rate of about 260 kg/s/m (overprediction of a factor of 15, Table 2). The damping effects can also be modeled by using a Munk–Anderson type of damping factor (see Table 2) related to the flux Richardson number Ri (van Rijn 2005) which is based on the velocity and concentration gradients. This method produces, however, insufficient damping in the near-bed layer (Fig. 13), because the concentration gradients near the bed and thus the Ri values (in the range of 0.01–0.1) are relatively small due to the hindered settling effects in case of large concentrations.

The damping effects can be best modeled by using a κ-epsilon modeling approach. The $c_{3\varepsilon}$ coefficient of the sediment-related dissipation term was set to −1.4 (Burchard and Baumert 1995) to simulate the additional dissipation of turbulent energy by the sediment particles. The computed velocity (based on cross-section averaged velocity of 2.05 m/s) and concentration profiles for Run S-15, shown in Fig. 13, are in good agreement (near-bed velocities about 10–20% too large) with the measured values. Finally, the empirical damping function proposed by van Rijn (1984b) is discussed. In the case of a pure sand bed the damping function reads as ($c_{\text{gel},s}=0.65$= maximum bed concentration)

$$\phi_d = 1 + (c/c_{\text{gel},s})^{0.8} - 2(c/c_{\text{gel},s})^{0.4} \quad \text{for } d_{50} \geq 1.5d_{\text{sand}} \qquad (15a)$$

Using Eq. (15*a*), the suspended transport is about 15 kg/s/m for Run S-15 of Einstein and Chien (1955), which is of the right order of magnitude. In the case of a silt–sand mixture with relatively large sediment suspensions and the presence of wash load, the damping effect will be somewhat larger. Based on analysis of the Huanghe River dataset (see below), it was found that

$$\phi_d = \phi_{fs}[1 + (c/c_{\text{gel},s})^{0.8} - 2(c/c_{\text{gel},s})^{0.4}] \qquad (15b)$$

where $\phi_{fs}=d_{50}/(1.5d_{sand})$=additional calibration factor and $\phi_{fs}=1$ for $d_{50}\geq 1.5d_{sand}$. When wash load is present, the turbulence damping is affected by both the wash load and the suspended sand load. The damping coefficient should be based on the total sediment concentration (sand+wash load concentration).

Summarizing, it is concluded that turbulence damping and hindered settling are both important effects, which cannot be neglected when the upper flow regime is considered. The inclusion of hindered settling alone leads to severe overestimation of the concentrations near the bed, whereas the inclusion of turbulence damping alone results in underestimation of the near-bed concentrations. Neglecting both effects leads to a systematic overestimation by a factor of maximum 3 for extreme flow conditions. The effect of sediment stratification on the velocity profiles can be most easily represented by introducing an apparent bed roughness of the order of the thickness of the sheet flow layer (about 100 d_{50}). The effect of sediment stratification on the concentration profile can be sufficiently accurate represented by an empirical damping function. The κ-epsilon model offers the best overall solution, but is not efficient for implementation in morphological models involving an almost infinite number of transport computations and bed updates over a large spatial domain. The effect of the sediment stratification on the overall flow resistance is not yet clear. The flow resistance decreases due to damping of turbulence, but it increases because the flow has to carry a larger sediment load. The experimental results of Einstein and Chien (1955) and those of Winterwerp et al. (1990) suggest that the overall roughness is somewhat larger due to the presence of a large sediment load (van Rijn 1993) compared to the roughness in a similar clear water flow.

Computation of Suspended Sand Transport

The current-related suspended sand transport can be determined from

$$q_{s,c} = \int_a^h ucdz \qquad (16)$$

where c=concentration profile, u=velocity profile including wave–current interaction effects (van Rijn 1993). Eq. (16) requires numerical integration. The simplified suspended load transport formula for steady flow proposed by van Rijn (1984b) was extended to coastal flow (waves) as (see also Soulsby 1997)

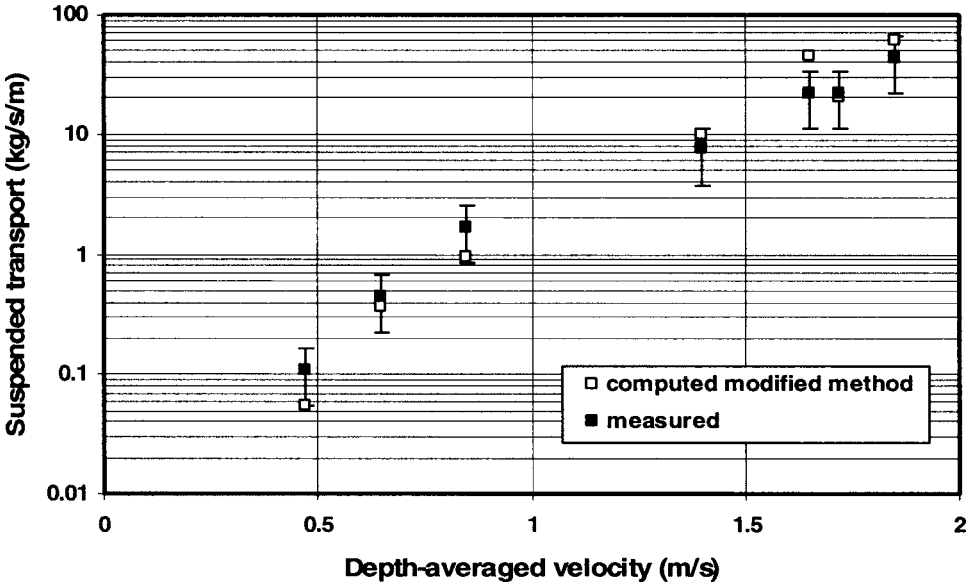

Fig. 14. Computed and measured suspended transport for Huanghe River, China (60–100 μm bed)

$$q_{s,c} = 0.012\rho_s u d_{50} M_e^{2.4} (D_*)^{-0.6} \tag{17}$$

with: $q_{s,c}$=suspended load transport (kg/s/m); h=water depth; d_{50}=particle size (m); $D_* = d_{50}[(s-1)g/\nu^2]^{1/3}$=dimensionless particle size; $s=\rho_s/\rho_w$=relative density; ν=kin viscosity; $M_e=(u_e-u_{cr})/[(s-1)gd_{50}]^{0.5}$=mobility parameter; u_e=effective velocity; and u_{cr}=critical depth-averaged velocity for initiation of motion. Eq. (17) shows that the current-related suspended transport is related to $d_{50}^{-0.8}$, which is a weaker influence compared with Eq. (1) based on field data. As a result, the suspended transport of very fine sediments (<0.1 mm) will be somewhat underestimated by Eq. (17).

Equation (16) defines the current-related suspended transport ($q_{s,c}$) which is the transport of sediment by the mean current including the effect of wave stirring on the sediment load. In the presence of surface waves an additional suspended transport component in the direction of the wave motion is generated as a result of the asymmetric oscillatory wave motion near the bed in shoaling waves. This type of suspended transport is defined as the wave-related suspended transport ($q_{s,w}$) and reads as (Houwman and Ruessink 1996; Grasmeijer et al. 1999; Grasmeijer 2002; van Rijn 2000)

$$q_{s,w} = \gamma V_{\text{asym}} \int_a^{\delta} c dz \tag{18}$$

where $V_{\text{asym}}=[(U_{\text{on}})^4-(U_{\text{off}})^4]/[(U_{\text{on}})^3+(U_{\text{off}})^3]$=velocity asymmetry factor (based on Houwman and Ruessink 1996); U_{on}=onshore-directed peak orbital velocity (based on method of Isobe and Horikawa 1982); U_{off}=offshore-directed peak orbital velocity; δ=thickness of suspension layer near the bed (=$3\delta_s$), see Eq. (3); and γ=0.1=phase factor. Eq. (18) represents the wave-related suspended transport, which can be in or against the wave direction depending on the bed form dimensions and the strength of the asymmetric wave motion. Nielsen (1988, 1992), Dohmen-Janssen (1999), O'Donoghue et al. (2004), and Van der Werf (2006) have shown that the net suspended transport can be against the wave propagation direction. However, this effect was mainly observed under regular waves with very pronounced ripples. Grasmeijer et al. (1999) and Grasmeijer (2002) have measured the net suspended transport rates using sophisticated acoustic instruments under irregular waves in a large-scale laboratory flume (Delta flume) and in the surf zone of Egmond Beach (The Netherlands). Two types of sediment beds were used in the Delta flume (160 and 330 μm). The water depth of the flume experiments was about 4.5 m, significant wave heights were in the range of 1–1.5 m, and ripples were present on the bed. Negative (offshore-directed) transport rates were not observed in these tests. The net wave-related suspended transport which occurred in a layer of about 10 ripple heights (about 0.3 m) was always positive and can be represented by a constant phase factor γ=0.1. A slightly smaller value was found to be valid for the surf zone of Egmond γ=0.05 (Grasmeijer 2002). Both experiments yield a very consistent trend with positive, onshore-directed suspended transport rates under irregular waves for sediments in the range of 160–330 μm. The γ factor used in the model includes the phase function proposed by Dohmen-Janssen (1999). The phase γ factor which depends on the parameter $p=(\delta_w)/(Tw_s)$ with δ_w=thickness of wave boundary layer, T=wave period, and w_s=fall velocity, has been modified so that it can produce negative transport rates (offshore directed) in the case of a rippled bed. The γ factor is an input switch (either constant or related to the phase lag parameter p). This approach is tested later on (other paper). Simulation of two large-scale laboratory events of nearshore bar behavior shows, however, that offshore-directed transport rates may not be very realistic under irregular waves over a rippled bed.

Recalibration of Suspended Transport Model

River Flow

The proposed numerical method (TR2004 model) has been tested extensively for river flow over sediment beds with $d_{50}>100$ μm (van Rijn 1984a,b,c, 1993). However, detailed sediment transport data of fine sediment beds (<100 μm) were not available in the open literature at that time. Van den Berg and Van Gelder (1993) performed detailed measurements in a

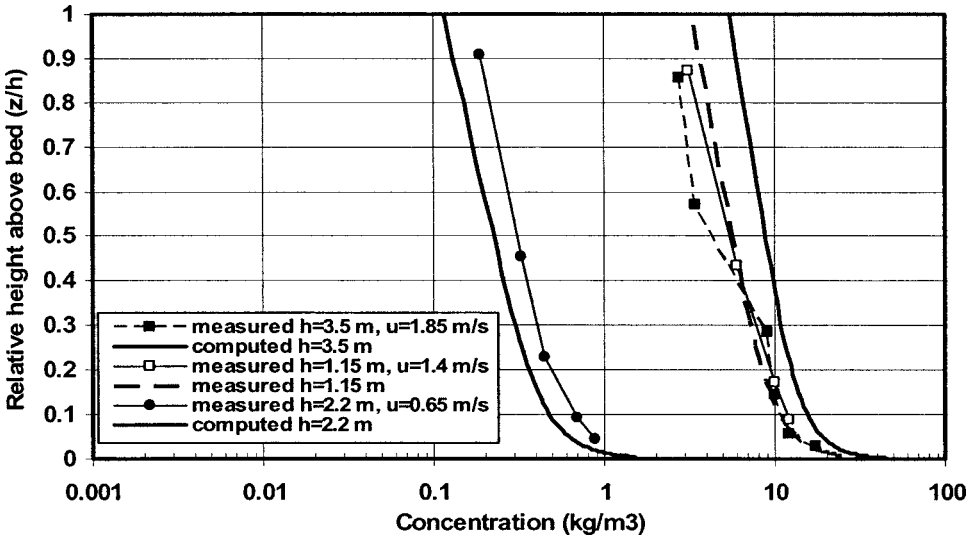

Fig. 15. Computed and measured concentration profiles for three cases $h=3.5$, 1.15, and 2.2 m

cross section of the Huanghe River (Yellow River) near the village of Li-Jin (about 100 km from the sea) in China. The Huanghe River in China is quite different from many rivers in the world. A unique feature is the high sediment load up to the hyperconcentration range (>100 kg/m^3) that frequently occurs during major floods. The suspended sediment load in the upper regime during major floods generally consists of 30–50% of fine sand (>62 μm), 30–60% of silt (8–62 μm), and 10–20% of clay (<8 μm), (Xu 1999a,b). The alluvial bed in the lower reach (length of about 1,000 km; east of Zhengzhou, China) dominantly consists of fine sand (62–125 μm). A pump sampler was used to determine the suspended sediment concentrations. In all, 13 detailed measurements of flow velocities, sediment concentrations, and particle sizes were completed. Herein, this data set was clustered into seven cases (see Table 3; other data $d_{10}=32$ μm, $T=24°$C, $I_b=$slope$=0.00015$). The suspended sediment contains a large fraction finer than 32 μm, which forms only a minor constituent of the bed material. Therefore, this fraction was defined as wash load and excluded from the concentration data. The wash load is 2–3 times as large as the sand load for high velocities and 5–20 times as large for low velocities (see Table 3).

The TR2004 model, including the bed roughness predictor, was used to compute the suspended transport for the 7 cases of Table 3. Most predicted transport rates are within a factor of 2 of the measured values (six out of seven cases). The computed suspended transport based on the original method [Eq. (15*a*), van Rijn 1984b] is somewhat too large for some cases (Cases 1+2 and Cases 5+6+7). As the predicted transport rates based on the original method are slightly too large, the turbulence damping coefficient was modified resulting in Eq. (15*b*). Most predicted values based on the modified method are within 50% of measured values. Computed and measured transport rates are shown in Fig. 14. Computed and measured concentration profiles for three cases are shown in Fig. 15. The vertical distribution as well as the magnitude of the concentrations are quite well represented.

Coastal Flow (Including Waves)

van Rijn (1993) calibrated the bed concentration [Eq. (5)] for coastal flow by introducing a wave-related efficiency factor (μ_w) in analogy with the current-related efficiency factor (μ_c). As much more field data sets have become available, the method is recalibrated. Furthermore, the model now includes a bed roughness predictor whereas earlier the bed roughness had to be estimated for each case from the available data. Therefore, the μ_w-factor was recalibrated using 54 data sets consisting of 21 laboratory tests and 33 field measurements (Tables 4 and 5). The depth-integrated suspended transport rates were available for 34 cases. These transport rates refer to the current-related suspended transport in the longshore direction. The Eg89 and E98

Table 4. Summary of Laboratory and Field Data of Coastal Sediment Transport

Source		Number of cases	Sediment size d_{50} (μm)	Water depth h (m)	Depth/mean velocity u (m/s)	Bed forms
Location	Reference					
DUT-F Delft University of Technology-Flume	van Rijn et al. (2001)	5	200	0.5	0.1–0.4	Ripples
V-B Vinje Basin Delft Hydraulics	van Rijn et al. (2001)	4	100	0.42	0.13–0.32	Ripples
DF1987, DF1997 Delta Flume Delft Hydraulics	van Rijn et al. (2001)	12	160–230	1–4.5	0	Ripples/flat
M73; Maplin Sands 1973 (U.K.)	Whitehouse et al. (1996)	6	140	3	0.1–0.3	Ripples
BP77; Boscombe Pier 1977 (U.K.)	Whitehouse et al. (1997)	5	250	5	0.2–0.4	Ripples
E89; E98; Egmond 1989 and 1998 (The Netherlands)	van Rijn et al. (2001)	14	300–350	1–3	0.1–0.5	Ripples
DS91; Duck Shelf 1991 (U.S.)	Madsen et al. (1993)	1	150	13	0.6	Ripples
N2003; Noordwijk 2003 (The Netherlands)	Grasmeijer et al. (2005b)	6	230	13–15	0.1–0.5	Ripples

Table 5. Summary of Laboratory and Field Data of Coastal Sediment Transport (Only Current-Related Suspended Transport; Longshore Suspended Transport)

Case	Water depth h (m)	Longshore velocity u_L (m/s)	Cross-shore velocity u_c (m/s)	Significant wave height H_s (m)	Peak wave period T_p (m)	Angle between current and wave direction [φ (degree)]	Sediment size			Temperature T (°C)	Salinity (parts per thousand)	Near-bed concentration at z		Suspended transport (kg/s/m)
							d_{10} (μm)	d_{50} (μm)	d_{90} (μm)			(m)	(kg/m^3)	
DUT628	0.52	—	0.093	0.121	2.5	0	140	205	300	17	0	0.34	0.017	0.00048
DUT630	0.51	—	0.22	0.123	2.6	0	140	205	300	17	0	0.35	0.019	0.002
DUT632	0.51	—	0.44	0.119	2.5	0	140	205	300	17	0	1.15	0.017	0.027
DUT635	0.5	—	0.107	0.146	2.4	0	140	205	300	17	0	0.59	0.019	0.00086
DUT637	0.51	—	0.22	0.151	2.4	0	140	205	300	17	0	0.81	0.022	0.0051
VB832	0.42	—	0.245	0.105	2.2	90	75	100	130	12	0	1.24	0.027	0.021
VB834	0.42	—	0.13	0.133	2.2	90	75	100	130	12	0	2.26	0.026	0.0122
VB835	0.42	—	0.256	0.139	2.3	90	75	100	130	12	0	3.26	0.024	0.047
VB836	0.42	—	0.317	0.137	2.2	90	75	100	130	12	0	4.0	0.024	0.098
DF87-2B	2.1	—	0	0.3	5.1	0	155	210	280	7	0	0.42	0.035	—
DF87-2C	2.1	—	0	0.4	5.1	0	155	210	280	7	0	1.1	0.03	—
DF87-2E	2.1	—	0	0.75	5.1	0	155	210	280	7	0	1.8	0.05	—
DF87-2F	2.1	—	–0.1	1.1	5.1	0	155	210	280	7	0	0.7	0.03	—
DF87-2G	2.2	—	–0.2	0.75	5	0	155	210	280	7	0	1.25	0.05	—
DF87-2H	1.41	—	–0.3	1.1	5.4	0	155	210	280	7	0	0.96	0.05	—
DF87-2I	1.13	—		1.1	5.4	0	155	210	280	7	0	2.53	0.05	—
DF97-1A	4.55	—	0	1	5	0	135	330	800	18	0	1.2	0.065	—
DF97-1B	4.55	—	0	1.25	5	0	135	330	800	18	0	1.55	0.065	—
DF97-1C	4.5	—	0	1	5	0	85	160	300	18	0	0.8	0.065	—
DF97-1D	4.5	—	0	1.25	5	0	85	160	300	18	0	1.3	0.065	—
DF97-1E	4.5	—	0	1.6	5	0	85	160	300	18	0	1.47	0.065	—
M73-0301	2.9	0.07	0	0.41	2.9	15	89	140	300	10	30	0.04	0.1	0.0011
M73-0302	3.15	0.24	0	0.42	3.1	15	89	140	300	10	30	0.1	0.1	0.016
M73-1301	3.03	0.135	0	0.42	3.2	15	89	140	300	10	30	0.174	0.1	0.0094
M73-1904	2.9	0.335	0	0.9	3.2	15	89	140	300	10	30	0.9	0.1	0.435
M73-2401	2.80	0.035	0	0.75	3	15	89	140	300	10	30	0.97	0.1	0.01
M73-2403	3.2	0.085	0	0.75	3.1	15	89	140	300	10	30	0.43	0.1	0.015
BP77-1	4.8	0.21	0	0.45	7.2	150	140	250	450	7	30	0.025	0.08	0.0024
BP77-2	5	0.42	0	0.55	6.7	150	140	250	450	7	30	0.076	0.1	0.022
BP77-3	4.9	0.24	0	0.95	6.8	150	140	250	450	7	30	0.43	0.08	0.055
BP77-4	5	0.3	0	1	6.6	150	140	250	450	7	30	0.84	0.05	0.08
BP77-5	5.3	0.4	0	1.05	6.5	150	140	250	450	7	30	1.05	0.05	0.3
E89-3C	1.1	0.24	–0.1	0.33	3.3	90	150	300	600	10	30	0.52	0.057	0.012

Table 5. (*Continued.*)

Case	Water depth h (m)	Longshore velocity u_L (m/s)	Cross-shore velocity u_c (m/s)	Significant wave height H_s (m)	Peak wave period T_p (m)	Angle between current and wave direction [φ (degree)]	Sediment size			Temperature T (°C)	Salinity (parts per thousand)	Near-bed concentration at z		Suspended transport (kg/s/m)
							d_{10} (μm)	d_{50} (μm)	d_{90} (μm)			(m)	(kg/m^3)	
E89-3D	1.05	0.06	−0.15	0.23	3.3	90	150	300	600	10	30	0.29	0.03	0.0025
E89-3E	1.12	0.55	−0.35	0.62	4	90	150	300	600	10	30	3.6	0.04	0.35
E89-4A	1.3	0.12	−0.1	0.7	7	90	155	350	800	10	30	1.0	0.045	0.07
E89-4B	1.3	0.35	−0.35	0.65	7	90	155	350	800	10	30	2.2	0.04	0.35
E89-4C	1.35	0.35	−0.1	0.6	5.5	90	155	350	800	10	30	0.72	0.057	0.05
E89-4E	1.3	0.2	−0.1	0.85	7.3	90	155	350	800	10	30	3.5	0.052	0.25
E89-4G	1.6	0.45	−0.3	0.9	7	90	155	350	800	10	30	3.3	0.038	0.5
E98-1	3.14	0.15	0.01	0.46	6.8	75	125	250	500	7	30	0.047	0.1	0.008
E98-2	2.71	0.15	−0.03	0.58	6.5	72	125	250	500	7	30	0.19	0.1	0.008
E98-3	2.87	0.17	−0.07	0.8	6.2	71	125	250	500	7	30	0.33	0.1	0.013
E98-4	2.54	0.16	−0.08	0.86	6.8	71	125	250	500	7	30	0.51	0.1	0.037
E98-5	2.7	0.28	−0.15	1.08	6.6	71	125	250	500	7	30	0.72	0.1	0.072
E98-6	2.13	0.28	−0.28	1.1	7.2	77	125	250	500	7	30	1.78	0.1	0.148
N2003-2200	15	0.32	0	2.25	7.2	100	150	220	440	10	30	0.1	0.15	—
N2003-2206	13.4	0.47	0	2.43	7.5	77	150	220	440	10	30	0.45	0.085	—
N2003-2205	13.6	0.46	0	2.4	7.3	75	150	220	440	10	30	0.23	0.12	—
N2003-2208	13.4	0.31	0	2.43	7.7	80	150	220	440	10	30	0.4	0.043	—
N2003-2209	13.3	0.2	0	2.8	8.1	82	150	220	440	10	30	0.47	0.021	—
N2003-2210	13.4	0.07	0	2.42	8.5	84	150	220	440	10	30	0.44	0.024	—
DS1991	13	0.6	0	3.75	11	80	80	150	300	15	30	2.5	0.54	—

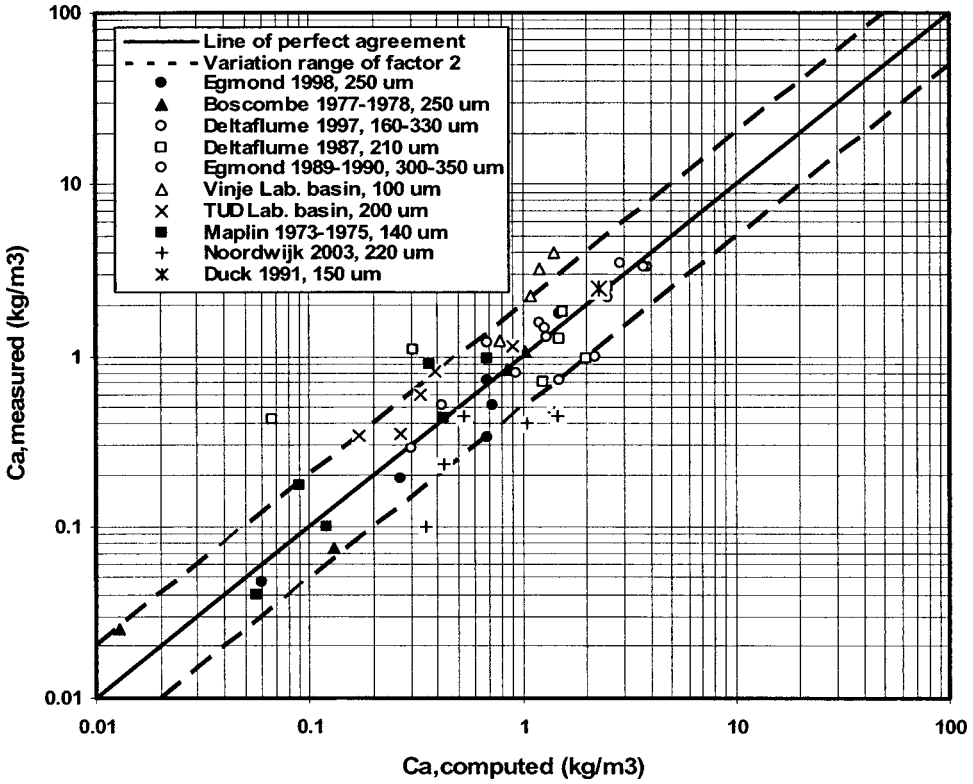

Fig. 16. Measured and computed reference concentrations for 54 cases

data refer to strongly breaking waves in the surf zone of Egmond (The Netherlands). The concentration measured in the lowest measurement point above the bed is herein defined as reference concentration and has been used to recalibrate the μ_w factor [see Eq. (5)]. The recalibrated μ_w factor is quite close to that proposed in 1993 [see Eq. (9)]. Fig. 16 shows measured and computed reference concentrations for 54 cases. About 70% of the computed cases are within a factor of 2 of measured values, which is a very reasonable result given the observed variability within the complete data set. Analysis of the available concentration profiles measured under similar conditions (same depth, sediment, velocity, and wave height) shows relatively large differences (up to a factor of 5) for some individual cases (Delft Hydraulics 2004). Comparison of measured and computed suspended transport also shows a score of 70% within a factor of 2.

Verification of Suspended Transport Model for River and Coastal Flow

Field data of measured suspended transport rates for river flow are presented in Figs. 2–4. The TR2004 model has been applied to compute the suspended transport for the three sediment classes, 100–200, 200–400, and 400–600 μm. It is assumed that $d_{10}=0.5d_{50}$ and $d_{90}=2d_{50}$ for all cases. The water depth is taken as $h=8$ m for Sediment Class 100–200 μm; the d_{50} is taken as 150 μm for $u=0.4-1$ m/s and 180 μm for $u=1.2-2$ m/s in line with the measured data. The water depth is $h=6$ m and $d_{50}=250$ μm for Sediment Class 200–400 μm. The water depth is $h=8$ m and the $d_{50}=400$ μm for Class 400–600 μm. The temperature is set to 15°C. The roughness and suspended sand sizes are predicted by the model. The computed suspended transport rates are shown in Figs. 2–4. The computed suspended transport rates are in reasonably good agreement (within a factor of 2) with measured values for velocities in the range of 0.7–1.8 m/s. The computed values appear to be significantly too small for velocities in the range of 0.4–0.6 m/s. The discrepancies in the lower-velocity range may be related to the presence of selective transport processes because the finer fractions of the sand bed may be winnowed and more easily transported in suspension. The application of a multifraction model yields larger suspended transport rates at low velocities (see later on).

Field data sets of measured suspended transport for coastal flow (North Sea) have been collected by Grasmeijer et al. (2005b). The study area is located 2 km off the coast of The Netherlands. The tidal depths are in the range of 13–15 m, the tidal velocities are in the range of 0.15–0.5 m/s, and the d_{10}, d_{50}, and d_{90} of the bed material are 190, 230, and 310 μm. Suspended transport measurements were made (Autumn of 2003) between 0.01 and 1 m above the bed with a 4.5 MHz acoustic sand transport meter (ASTM) attached to an instrumented, stand-alone tripod. Herein, only the data with a significant wave height larger than 1 m are used (seven cluster cases with $H_s=2.3-3.1$ m). The ratio of computed and measured suspended transport rates are in the range of 0.4–2.5 (not shown). On average, the computed values are somewhat too large (factor of 1.3), (see Grasmeijer et al. 2005a). The computed suspended transport rates are much too small for three cases just beyond intitiation of motion. Better agreement was obtained for these cases using a multifraction approach with 10 fractions (see later on). The automatic selection of roughness and suspended size is a major advancement, as no user judgement is required.

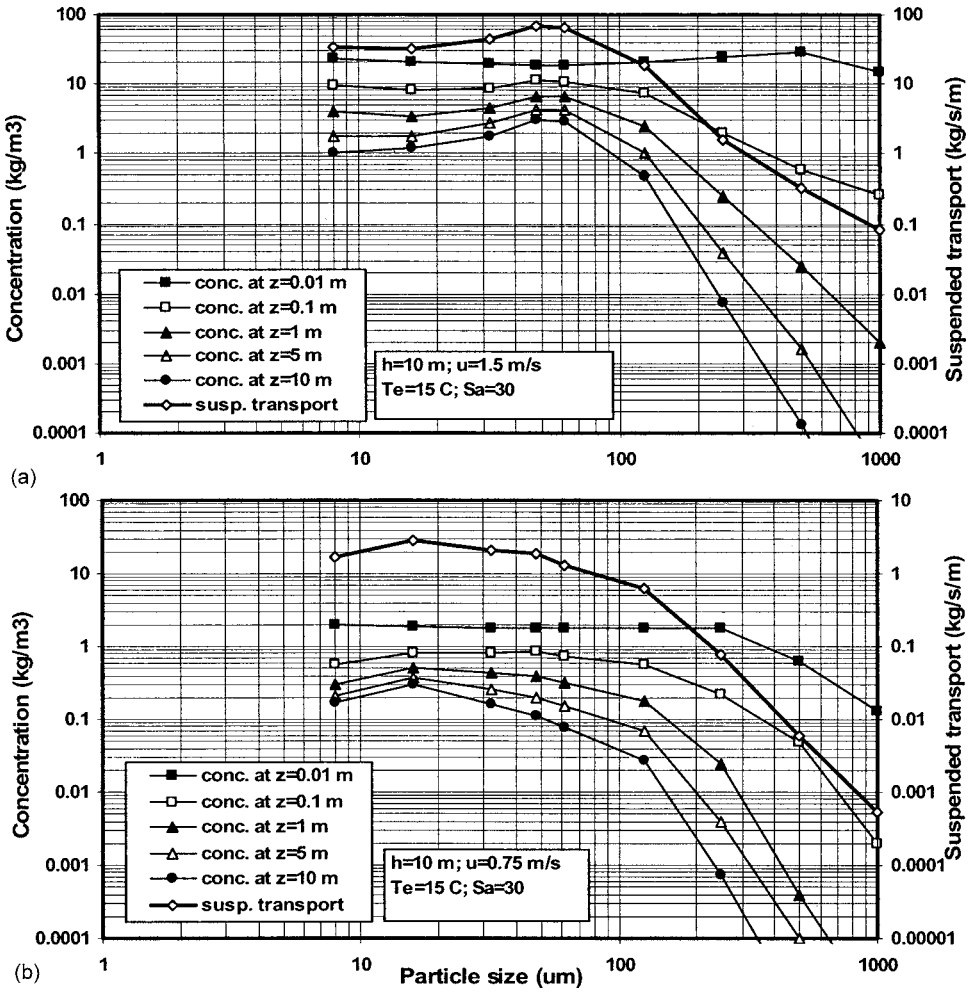

Fig. 17. Computed sediment concentration and suspended transport as function of particle size in saline conditions (Sa=30); depth-averaged velocity $u=1.5$ m/s (a); $u=0.75$ m/s (b)

Application of Sediment Transport Model

Steady River Flow over Fine Sediment Beds

The effect of sediment size on the concentrations and on the suspended transport was studied for a range of conditions: $d_{50}=8$, 16, 32, 48, 62, 125, 250, 500, and 1000 μm. The d_{10} was set to $0.5d_{50}$; d_{90} was set to $2d_{50}$. The depth-averaged velocity is 0.75 and 1.5 m/s. The water depth is $h=10$ m. Fresh (Sa=0) and saline (Sa=30) water have been used to study the effect of flocculation. The temperature is 15°C. Fig. 17 shows the computed concentrations at various elevations ($z=0.01$, 0.1, 5, and 10 m above the bed) as a function of size in saline conditions (Sa=30 ppt) based on a depth-averaged velocity of $u=0.75$ m/s [Fig. 17(b)] and $u=1.5$ m/s [Fig. 17(a)].

The following features can be observed:

$v=1.5$ m/s [Fig. 17(a)]:

- Near-bed concentration slightly increases from 15 to 30 kg/m^3 for particle sizes increasing from 8 to 500 μm and decreases for particle sizes larger than 500 μm;
- Decrease of the concentrations over the depth is minimum (factor of 5) for a particle size of 62 μm; the suspended transport is maximum for a particle size of 62 μm;
- Concentrations decrease over the depth at an increasing rate for particle sizes in the sand range (larger than 62 μm) due to the relatively large fall velocities; and
- Concentrations decrease over the depth at an increasing rate (factor of 15 for 8 μm) for particle sizes in the clay-silt range (smaller than 62 μm) due to the flocculation effect resulting in larger effective fall velocities

$v=0.75$ m/s [Fig. (17b)]

- Near-bed concentration is approximately constant (about 2 kg/m^3) for particle sizes increasing from 8 to 125 μm; and decreases for particle sizes large than 125 μm;
- Suspended transport is approximately constant for particle sizes smaller than about 48 μm; the concentrations show a decrease of a factor of 10–20 over the depth due to the flocculation effect; the flocculation effect is largest for a particle size of 8 μm; and
- Concentrations decrease over the depth at an increasing rate for particle sizes in the sand range (larger than 62 μm) due to the relatively large fall velocities.

At large velocities [Fig. 17(a)] the suspended transport increases as the particle size increases, reaches a maximum, and then decreases again for larger particle sizes. This behavior was also observed by Roberts et al. (1998) for the erosion of sediment

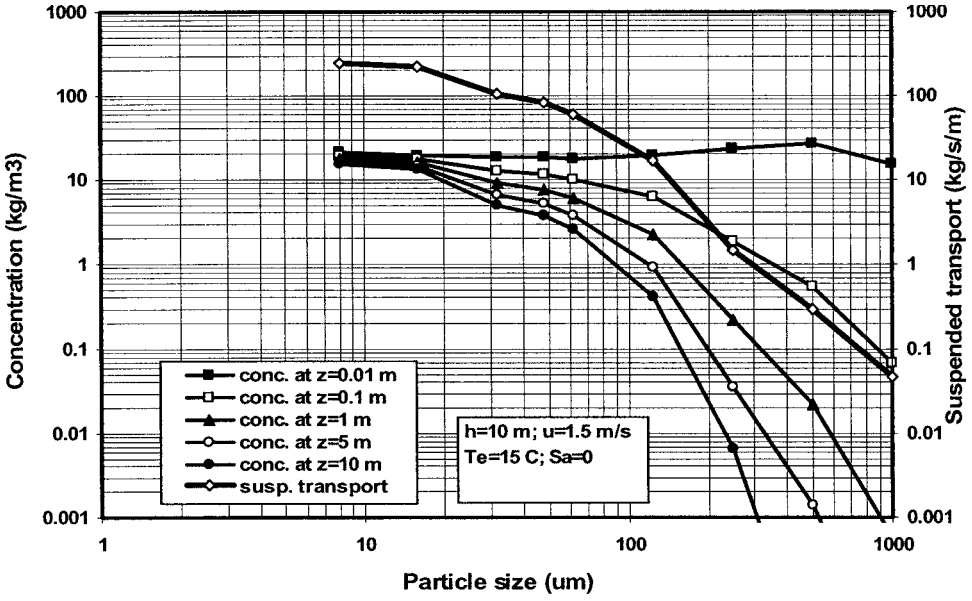

Fig. 18. Computed sediment concentration and suspended transport as function of particle size in fresh water conditions (Sa=0); depth-averaged velocity $u=1.5$ m/s

beds of 15–1,350 μm. Particles smaller than 32 μm were observed to behave in a cohesive manner, i.e., the particles consolidated slowly with time and were eroded in aggregates or chunks (mass erosion), which disintegrated as they were transported downstream.

Fig. 18 shows the computed concentration at various elevations as a function of particle size in fresh water conditions (Sa=0 ppt) based on a depth-averaged velocity of $u=1.5$ m/s. The computed concentrations and hence the suspended transport are maximum for a particle size of 8 μm. The concentrations are almost uniformly distributed over the depth for sizes smaller than 8 μm, because flocculation is assumed to be absent in fresh water flow. Hence, the suspended transport rates in the fine silt range (<20 μm) are much larger (factor of 8) than in saline water. This effect of salinity on the suspended transport rate is almost absent for particle size larger than 48 μm. Fig. 19 shows computed concentrations profiles for a size of 16 μm with and without flocculation. The concentrations are largest without flocculation. The near-bed concentrations are almost the same (about 20 kg/m^3).

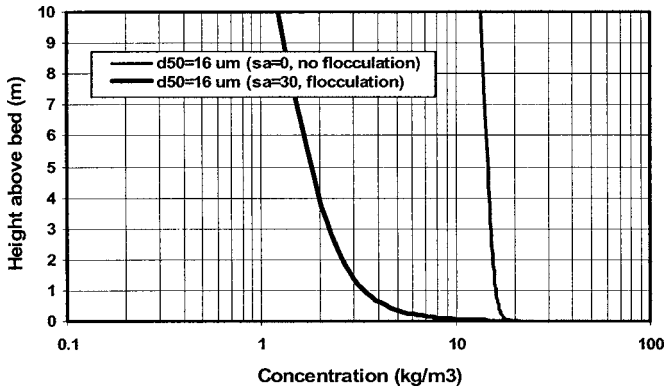

Fig. 19. Computed concentration profiles; particle size=16 μm, $u=1.5$ m/s, and $h=10$ m

A distinct two-layer system as observed by Shi and Zhou (2004) can be observed for flocculating conditions with concentrations in the range of 1–20 kg/m^3.

The concentrations computed by the TR2004 model for fine sediment beds in saline conditions are of the right order of magnitude compared with observed values in the Changjiang Estuary in China (Li 1991; Li et al. 1993, 2000; Shi and Zhou 2004). The near-bed concentrations at peak tidal flow are of the order of 2–10 kg/m^3 for the fine silty bed range (10–62 μm) and 5–20 kg/m^3 in the zone of the turbidity maximum, where fluid mud layers are a dominant phenomenon.

Steady Coastal Flow over Fine Sand Bed with and without Waves

The TR2004 model was used to compute the total sand transport rates in a depth of 5 m and a median size of $d_{50}=250$ μm ($d_{10}=125$ μm, $d_{90}=500$ μm). The wave height was varied in the range of 0–3 m and wave periods in the range of 5–8 s. The wave direction is assumed to be normal to the coast, whereas the current is assumed to be parallel to the coast ($\varphi=90°$). The temperature is 15°C and the salinity is 0. Both the bed roughness and the suspended size are predicted by the model. The total load transport (bed load+suspended load) results of the TR2004 model are shown in Fig. 20 together with earlier results of the TR1993 model (van Rijn 1993) for the same parameter range. The TR2004 model yields smaller transport rates (maximum factor of 2) for steady flow without waves and for steady flow with low waves ($H_s=0.5$ and 1 m), which is mainly caused by the smaller bed roughness values predicted by the TR2004 model. The TR1993 model results are based on assumed bed roughness values in the range of 0.1–0.02 m for velocities increasing from 0.1 to 2 m/s. The TR2004 model yields values in the range of 0.05–0.02 m. The TR2004 model yields slightly smaller transport rates for relatively high waves ($H_s=2$ and 3 m). The TR2004 results for steady flow (without waves) show good agreement with measured values (data from major rivers and estuaries with

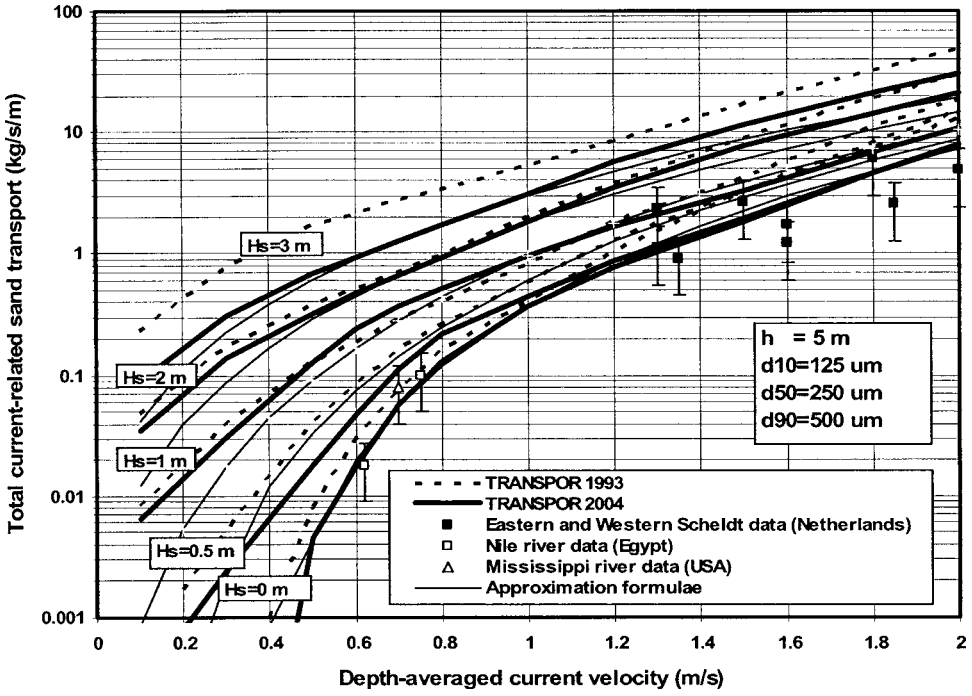

Fig. 20. Total sand transport for combined wave-current conditions, $h=5$ m, $d_{50}=250$ μm

depth of about 5 m and sediment size of about 250 μm) over the full velocity range from 0.6 to 2 m/s. The results of the TR2004 show that the total transport varies with u^5 for $H_s=0$ m, $u^{2.5}$ for $H_s=1$ m, and u^2 for $H_s=3$ m. The transport rate varies with H_s^3 for $u=0.5$ m/s, with $H_s^{1.5}$ for $u=1$ m/s and with H_s for $u=2$ m/s.

The total transport rate ($q_t=q_b+q_s$) based on the simplified method [Eq. (17)] is also shown in Fig. 20. Compared with the results of the TR2004 model, the approximation functions tend to overpredict (maximum factor of 2) for $u>$ approximately 0.6 m/s in the case of steady flow without waves and for low waves ($H_s=0.5$ and 1 m) and underpredict (maximum factor of 2) for relatively high waves ($H_s=2$ and 3 m) in combination with low or high velocities. The ratio of bed load transport and total load transport varies from 0.5 to 0.05 for $H_s=0$ and 0.5 m, from 0.2 to 0.02 for $H_s=1$ m and between 0.1 and 0.01 for $H_s=2$ and 3 m.

Wash Load

The transport of very fine sediments in conditions with almost uniform suspensions (often defined as wash load) can be described by energy-based methods, as proposed by Velikanov (see Chien 1998) and later by Bagnold (1962). The presence of wash load will have a significant effect on the bed material load due to hindered settling effects resulting in an increase of the bed material load. Bagnold (1962) derived the equilibrium or saturation sediment concentration (c_s) by considering the energy required to keep the sediment load in suspension and the energy dissipated by the transport of sediment. The energy (per unit time) required to keep the suspended load in suspension is

$$E_r = (\rho_s - \rho_w) g h (c_s/\rho_s) w_s \tag{19}$$

where c_s=equilibrium or saturation sediment concentration (mass); assumed to be uniform over depth; h=depth; and w_s=effective fall velocity of suspended sediment.

The energy dissipated by the flow in transporting sediments is given by

$$E_d = e_s(\tau_b u) \tag{20}$$

where e_s=efficiency coefficient (order of 0.025; Bagnold 1966); $\tau_b=\rho_m g u^2/C^2$=bed–shear stress; u=depth-averaged velocity; C=Chézy coefficient, $\rho_m=\rho_w(1+(s-1)c_s/\rho_s)$=mixture density.

Assuming $E_r=E_d$, yields

$$c_s = K\rho_s[(1+\alpha c_s)][u^3/(ghw_s)] \tag{21}$$

where $K=[(e_s g)/((s-1)C^2)]$; $s=\rho_s/\rho_w$=relative density (2.65 for quartz sediment in fresh water at 20°C); and $\alpha=(s-1)/\rho_s=0.00062$. Bagnold (1962) uses $K_b=(1-e_b)K$ with e_b=efficiency factor related to transport of bed load (=0.15). The K value is of the order of 0.000015 for $C=100$ m$^{0.5}$/s. Based on the concept of turbulence collapse in stratified flow, Winterwerp (2001) derived a similar expression for the saturation concentration with $K_w=0.7$ g$^{1.5}$/$[s(s-1)C^3]$.

Expression (21) yields a dual sediment concentration and hence transport capacity if the hindered settling effect is included. Using $w_s=(1-c_s/c_{\max})^5 w_{s,o}$ for fine sediment, the relationship between the saturation concentration (c_s) and depth-averaged velocity (u) can be expressed as

$$u=[(\rho_s K)^{-1}(c_s)(1+\alpha c_s)^{-1}(1-c_s/c_{\max})^5(ghw_{s,o})]^{0.3333} \tag{22a}$$

or in dimensionless form

$$u^3/(ghw_{s,o}) = [(\rho_s K)^{-1}(c_s)(1+\alpha c_s)^{-1}(1-c_s/c_{\max})^5] \tag{22b}$$

Eq. (22a) is shown in Fig. 21 for particle sizes of 8 to 32 μm using $s=2.65$, $h=10$ m, kinematic viscosity coefficient $=1\times10^{-6}$ m^2/s, $C=100$ m$^{0.5}$/s; fall velocity based on Stokes expression. The maximum bed concentration is assumed to be equal to the maximum hyperconcentration observed, which is

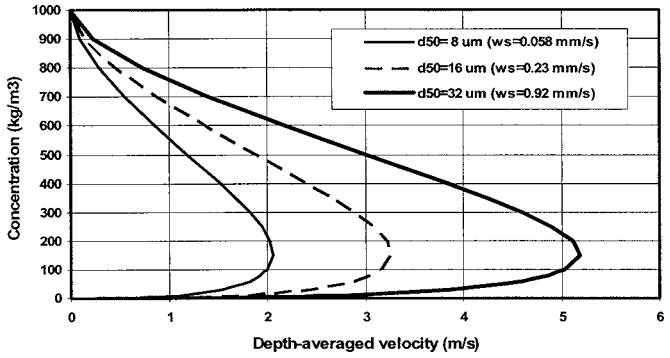

Fig. 21. Saturation concentration as function of depth-averaged velocity and particle size of fine sediments ($h=10$ m, $C=100$ m$^{0.5}$/s, $c_{max}=1{,}000$ kg/m^3, $v=10^{-6}$ m^2/s)

about $c_{max}=1{,}000$ kg/m^3 (Xu 1999a,b). Eq. (22*a*) or (22*b*) yields a dual saturation concentration (c_s) for a given depth-averaged velocity. The lower concentration is the sub-saturation value (maximum value of about 150 kg/m^3 for particles in the range of 8 to 32 μm; see Fig. 21) related to pickup of silt from the bed; the upper value is the absolute saturation concentration depending on the upstream supply rate; see Fig. 22. The maximum saturation concentration is also known as supersaturation or hyperconcentration. These high hyperconcentrations and associated transport capacity strongly depend on the hindered settling process and on the upstream supply rate rather than on the local bed material. The lower values (subsaturation range; minor hindered settling) can be transported by erosion of sediment from the local bed (in conditions with a low supply rate from upstream). Saturation concentrations of clay (8 μm) in the range of 1–150 kg/m^3 can be transported at velocities of 1–2 m/s. The transport of silt particles (32 μm) at concentrations of 1–150 kg/m^3 requires larger velocities in the range of 4–5 m/s. Eq. (22*b*) results in a collapse of the curves of Fig. 21 into one curve, shown in Fig. 22. Measured wash load concentration values and ranges for the Huanghe River in China (Xu 1999a,b; Van den Berg and Van Gelder 1993) are also shown. As regards the wash load data of Van den Berg and Van Gelder (1993), the suspended sediment is assumed to be 16 μm with $w_{s,o}=0.23$ mm/s. Remarkably good agreement between computed and measured values can be observed using a maximum concentration of 1,000 kg/m^3. Eq. (22*b*) can be used to estimate the saturation concentration of wash load consisting of sediments smaller than 32 μm in an alluvial river. Generally, this type of sediment does not occur in the main alluvial bed of the river. The mean particle size of the wash load will be somewhere in the range of 8–16 μm.

Assuming bed material of 16 μm, the TR2004 model based on Eqs. (2)–(16) yields saturation concentrations in the range of 3–100 kg/m^3 for depth-averaged velocities in the range of 1–3 m/s. These values are somewhat larger (factor of 2) than those of Eq. (22*a*). This part of the wash load can be seen as the local contribution. Hyperconcentrations cannot be predicted by the TR2004 model, because these types of concentrations are largely determined by the supply conditions (advective contribution from upstream). However, the fall velocity of the bed sediments (once suspended) will be significantly reduced when hyperconcentrations are present in the flow (hindered settling effects).

Conclusions

The findings of the present study can be summarized in the following conclusions:

- High-quality field data of river and coastal flows have been selected and clustered into four particle size classes (60–100, 100–200, 200–400, and 400–600 μm). The suspended sand transport is strongly dependent on particle size and on current velocity; the sand transport increases by a factor of about 500 for velocities increasing from 0.4 to 2 (velocity to power 3.5). The effect of water depth (between 1 and 15 m) on the sus-

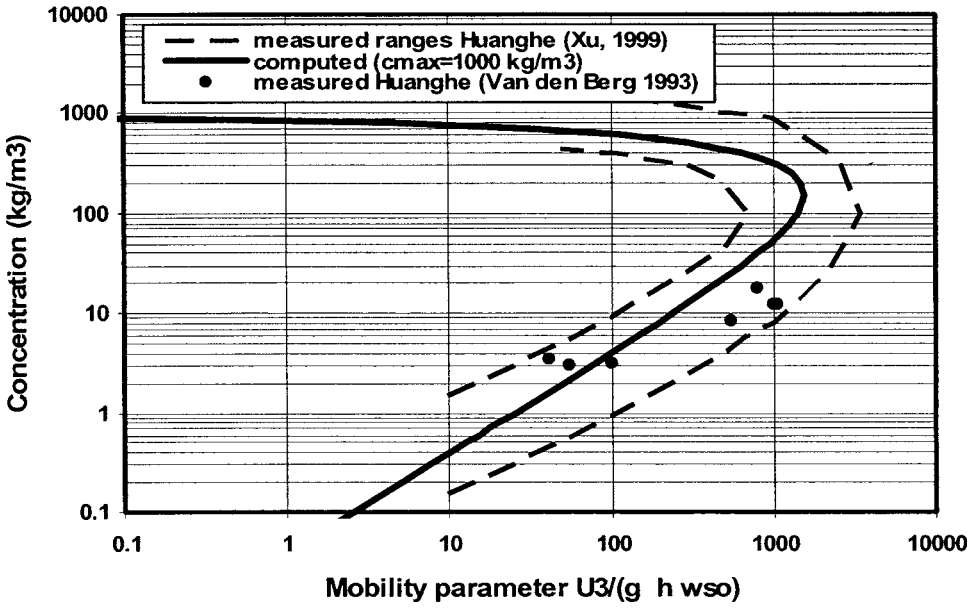

Fig. 22. Saturation concentration as function of dimensionless mobility parameter ($h=10$ m, $C=100$ m$^{0.5}$/s, $c_{max}=1{,}000$ kg/m^3, $v=10^{-6}$ m^2/s)

pended transport appears to be of minor importance; the field data can be represented by a simple function [Eq. (1)].

- Current-related (longshore) suspended sand transport in the coastal zone is found to be strongly dependent on the relative wave height (H_s/h), particularly for current velocities in the range 0.1–0.6 m/s. The transport of suspended sand in the size range 100–400 μm increases by a factor of 10–100 when waves are superimposed. The wave-related suspended transport may be in or against the wave direction; laboratory and field data under irrregular waves over sediment beds between 160 and 330 μm show a consistent net onshore-directed suspended transport, which can be represented by a fairly simple expression.
- Time-averaged (over the wave period) advection-diffusion equation is applied to compute the time-averaged sand concentration profile for combined current and wave conditions. Flocculation, hindered settling and turbulence damping effects are included by fairly simple expressions. The bed-shear stress is based on a new bed roughness predictor. The reference concentration function has been recalibrated using laboratory and field data for combined steady and oscillatory flow and is extended to the fine silt range (8–62 μm). The results for the sand range (≥62 μm) are close to earlier results.
- Computed current-related suspended transport rates show reasonably good agreement (within a factor of 2) with measured values for velocities in the range of 0.6–1.8. m/s and sediments in the range of 60–600 μm. The proposed single-fraction method underpredicts in the low velocity range. Much better agreement can be obtained by using a multifraction method in the low velocity range as the process of winnowing of fine sediments can be better represented.
- Proposed model has been used to explore the suspended sediment transport in the fine silt and sand range (8–100 μm) showing that flocculation effects are extremely important in tidal flow and that the suspended transport has a maximum for a particle size of about 62 μm.
- New simplified transport formula is presented, which can be used to obtain a quick estimate of current-related suspended transport; it may underestimate for very fine sediments (<100 μm) and for very small velocities (<0.6 m/s).
- Modeling of wash load transport in river flow based on the energy-concept of Bagnold (1962, 1966) shows that an extremely large amount (up to 1,000 kg/m^3) of very fine sediment can be transported by the flow.

The proposed TR2004 method needs further verification in the fine silt bed range (8–62 μm) using field data from major estuaries and in the cross-shore transport range using data from the inner surf and swash zone.

Acknowledgments

The National Institute for Coasts and Sea (RIKZ/Rijkswaterstaat, The Netherlands) is gratefully acknowledged for providing research funds within the Generic Coastal Research Program (VOP). Also acknowledged are the Basic Research Program of Delft Hydraulics and the European Research Projects SEDMOC, COAST3D, and SANDPIT sponsored by the European Community Research Programme. J. R. van den Berg and M. Kleinhans of the University of Utrecht are gratefully acknowledged for their critical comments on the manuscript.

References

Abdel-Fattah, S. (1997). "Field measurements of sediment load transport in the Nile River at Sohag." *Technical Rep.*, Hydraulics Research Institute, Delta Barrage, Egypt.

Bagnold, R. A. (1962). "Autosuspension of transported sediment; turbidity currents." *Proc. R. Soc. London, Ser. A*, 265, 315–319.

Bagnold, R. A. (1966). "An approach to the sediment transport problem from general physics." *Geological Survey Professional Paper 422-I*, U.S. Geological Survey, Reston, Va.

Bijker, E. W. (1971). "Longshore transport computations." *J. Wtrwy., Harb. and Coast. Engrg. Div.*, 99(4), 687–701.

Burchard, H., and Baumert, H. (1995). "On the performance of a mixed-layer model-based on the κ-ε turbulence closure." *J. Geophys. Res.*, 100(5), 8523–8540.

Chien, N., and Wan, Z. (1999). *Mechanics of sediment transport*, ASCE, Reston, Va.

Coleman, N. L. (1970). "Flume studies of the sediment transfer coefficient." *Water Resour. Res.*, 6(3), 801–809.

Culbertson, J. K., Scott, C. H., and Bennet, J. P. (1972). "Summary of alluvial channel data from Rio Grande Conveyance Channel, New Mexico, 1965–1969." *Geological Survey Professional Paper 562-J*, U.S. Geological Survey, Reston, Va.

Delft Hydraulics. (1985). "Sand transport at high velocities." *Rep. M2127*, Delft Hydraulics, Delft, The Netherlands.

Delft Hydraulics. (2004). "Description of TRANSPOR2004 and implementation in DELFT3D online." *Rep. Z3748*, Delft Hydraulics, Delft, The Netherlands.

Dohmen-Janssen, M. (1999). "Grain size influence on sediment transport in oscillatory sheet flow." Doctoral thesis. Dept. of Civil Engineering, Univ. of Twente, Enschede, The Netherlands.

Einstein, H. A., and Chien, N. (1955). "Effects of heavy sediment concentration near the bed on velocity and sediment distribution." *M.R.D. sediment series no. 8*, Univ. of California at Berkeley, Berkeley, Calif.

Grasmeijer, B. T. (2002). "Process-based cross-shore modeling of barred beaches." Doctoral thesis, Dept. of Physical Geography, Univ. of Utrecht, Utrecht, The Netherlands.

Grasmeijer, B. T., Chung, D. H., and van Rijn, L. C. (1999). "Depth-integrated sand transport in the surf zone." *Proc., Coastal Sediments*, ASCE, Reston, Va., 325–340.

Grasmeijer, B. T., Davies, A. G., Guizien, K., Van der Werf, J. J., van Rijn, L. C., Walther, R., Sutherland, J., and Biegowski, J. (2005a). "Intercomparison results of sand transport models." *Sand transport and morphology of offshore mining pits (SANDPIT Project)*, L. C. van Rijn, R. L. Soulsby, P. Hoekstra, and A. G. Davies, eds., Aqua, Amsterdam, The Netherlands, AM1–AM10.

Grasmeijer, B. T., Dolphin, T., Vincent, C., and Kleinhans, M. G. (2005b). "Suspended sand concentrations and transports in tidal flow with and without waves." *Sand transport and morphology of offshore mining pits (SANDPIT Project)*, L. C. van Rijn, R. L. Soulsby, P. Hockstra, and A. G. Devies, eds., Aqua, Amsterdam, The Netherlands, U1–U13.

Grasmeijer, B. T., and van Rijn, L. C. (2001). "Sand transport in the surf zone of a dissipative beach." *Proc., Coastal Dynamics*, ASCE, Reston, Va., 102–111.

Houwman, K. T., and Ruessink, B. G. (1996). "Sediment transport in the vicinity of the shoreface nourishment of Terschelling." *Rep.*, Dept. of Physical Geography, Univ. of Utrecht, Utrecht, The Netherlands.

Isobe, M., and Horikawa, K. (1982). "Study on water particle velocities of shoaling and breaking waves." *Coast. Eng. Japan*, 25, 109–123.

Kleinhans, M. G. (1999). "Sediment transport in River Waal, The Netherlands." *Rep. ICG 99/6*, Dept. of Physical Geography, Univ. of Utrecht, Utrecht, The Netherlands.

Kroon, A. (1994). "Sediment transport and morphodynamics of the beach and nearshore zone near Egmond, The Netherlands." Doctoral thesis, Dept. of Physical Geography, Univ. of Utrecht, Utrecht, The Netherlands.

Li, J. (1991). "The rule of sediment transport on the Nanhui tidal flat in

the Changjiang Estuary." *Acta Oceanol. Sinica*, 10(1), 117–127.
Li, J., Qing, H. Q., Zhang, L., and Shen, H. (2000). "Sediment deposition and resuspension in mouth bar area of the Yangtze Estuary." *China Ocean Eng.*, 14(3), 339–348.
Li, J., Shi, W., Shen, H., Xu, H., and Eisma, D. (1993). "The bed load movement in the Changjiang Estuary." *China Ocean Eng.*, 7(4), 441–450.
Li, J., Wan, X.-N., He, Q., Ying, M., Shi, L.-Q., and Hutchinson, S. M. (2004). "In situ observation of fluid mud in the north passage of Yangtze Estuary, China." *China Ocean Eng.*, 18(1), 149–156.
Madsen, O. S., Wright, L. D., Boon, J. D., and Chisholm, T. A. (1993). "Wind stress, bed roughness, and sediment suspension on the inner shelf during an extreme storm event." *Cont. Shelf Res.*, 13(11), 1303–1324.
McNown, J. S., and Lin, P. N. (1952). "Sediment concentration and fall velocity." *Proc., 2nd Mid Western Conf. on Fluid Mechanics*, Ohio State Univ., 401–411.
Nielsen, P. (1988). "Three simple models of wave sediment transport." *Coastal Eng.*, 10, 43–62.
Nielsen, P. (1991). "Combined convection diffusion: A new framework for suspended sediment modelling." *Proc., Coastal Sediments*, Seattle, ASCE, Reston, Va., 418–431.
Nielsen, P. (1992). *Coastal bottom boundary layers and sediment transport*, World Scientific, Singapore.
Nielsen, P., and Teakle, I. A. L. (2004). "Turbulent diffusion of momentum and suspended particles: A finite-mixing length theory." *Phys. Fluids*, 16(7), 2342–2348.
Oliver, D. R. (1961). "The sediment suspension of closely-spaced spherical particles." *Chem. Eng. Sci.*, 15, 230–242.
O'Donoghue, T., Li, M., Malarkey, J., Pan, S., Davies, A. G., and O'Connor, B. A. (2004). "Numerical and experimental study of wave-generated sheet flow." *Proc., 29th Int. Conf. on Coastal Engineering*, Lisbon, 1690–1702.
Peterson, A. W., and Howells, R. F. (1973). "Compendium of solids transport data for mobile boundary data." *Rep. HY-1973-ST3*, Dept. of Civil Eng., Univ. of Alberta, Alberta, Ont., Canada.
Richardson, J. F., and Meikle, R. A. (1961). "Sedimentation and fluidization: Part II." *Trans. Inst. Chem. Eng.*, 39, 348–356.
Richardson, J. F., and Zaki, W. N. (1954). "Sedimentation and fluidization: Part I." *Trans. Inst. Chem. Eng.*, 32, 35–50.
Roberts, J., Jepsen, R., Gotthard, D., and Lick, W. (1998). "Effects of particle size and bulk density on erosion of quartz particles." *J. Hydraul. Eng.*, 124(12), 1261–1267.
Scott, C. H., and Stephens, H. D. (1966). "Special sediment investigation, Mississippi River at St. Louis, Missouri, 1961–1963." *Geological Survey Water Supply Paper 1819-J*, U.S. Geological Survey, Reston, Va.
Shi, Z., and Zhou, H. J. (2004). "Controls on effective settling velocities of mud flocs in the Changjiang Estuary, China." *Hydrolog. Process.*, 18, 2877–2892.
Sistermans, P. G. J. (2002). "Graded sediment transport by nonbreaking waves and a current." Doctoral thesis, Dept. of Civil Engineering, Delft Univ. of Technology, Delft, The Netherlands.
Soulsby, R. (1997). *Dynamics of marine sands*, Thomas Telford, London.
Thorn, M. F. C. (1981). "Physical processes of siltation in tidal channels." *Proc., Hydraulic Modeling of Maritime Engineering Problems*, Institution of Civil Engineers, London, 47–55.
Van den Berg, J. H., and Van Gelder, A. (1993). "Prediction of suspended bed material transport in flows over silt and very fine sand." *Water Resour. Res.*, 29(5), 1393–1404.
Van der Werf, J. J. (2006). "Sand transport over rippled beds in oscillatory flow." Doctoral thesis, Dept. of Civil Engineering, Univ. of Twente, Enschede, The Netherlands.
van Rijn, L. C. (1984a). "Sediment transport. Part I: Bed load transport." *J. Hydraul. Eng.*, 110(10), 1431–1456.
van Rijn, L. C. (1984b). "Sediment transport. Part II: Suspended load transport." *J. Hydraul. Eng.*, 110(11), 1613–1641.
van Rijn, L. C. (1984c). "Sediment transport. Part III: Bed forms and alluvial roughness." *J. Hydraul. Eng.*, 110(12), 1733–1754.
van Rijn, L. C. (1987). "Mathematical modeling of morphological processes in the case of suspended sediment transport." Doctoral Thesis. Dept. of Fluids Mechanics, Delft Univ. of Technology, Delft, The Netherlands.
van Rijn, L. C. (1993). *Principles of sediment transport in rivers, estuaries, and coastal seas*, Aqua, Blokzijl, The Netherlands.
van Rijn, L. C. (2000). "General view on sediment transport by currents and waves." *Rep. Z2899*, Delft Hydraulics, Delft, The Netherlands.
van Rijn, L. C. (2005). *Principles of sedimentation and erosion engineering in rivers, estuaries, and coastal seas*, Aqua, Blokzijl, The Netherlands.
van Rijn, L. C. (2007). *Principles of sediment transport in rivers, estuaries, and coastal ses* (Update/supplement), Aqua, Blokzijl, The Netherlands, ⟨www.aquapublications.nl⟩.
van Rijn, L. C., Grasmeijer, B. T., and Sistermans, P. (2001). *SEDMOC database*, Delft Hydraulics, Delft, The Netherlands.
Vanoni, V. A. (1977). *Sedimentation engineering*, ASCE, New York.
Vinzon, S. B., and Mehta, A. J. (2003). "Lutoclines in high concentration estuaries: Some observations at the mouth of the Amazon." *J. Coastal Res.*, 19(2), 243–253.
Voogt, L., van Rijn, L. C., and Van den Berg, J. H. (1991). "Sediment transport of fine sands at high velocities." *J. Hydraul. Eng.*, 117(7), 869–890.
Whitehouse, R. J., Owen, M. W., and Stevenson, E. C. (1997). "Sediment transport measurements at Boscombe Pier, Poole Bay." *Rep. TR 27*, Wallingford, U.K.
Whitehouse, R. J., Thorn, M. F. C., and Houghton, P. J. (1996). "Sediment transport measurements at Maplin Sands, Outer Thames Estuary." *Rep. TR 15*, Wallingford, U.K.
Winterwerp, J. C. (1999). "On the dynamics of high-concentrated mud suspensions." Doctoral thesis, Dept. of Civil Engineering, Delft Univ. of Technology, Delft, The Netherlands.
Winterwerp, J. C. (2001). "Stratification effects by cohesive and noncohesive sediment." *J. Geophys. Res.*, 106(10), 22559–22574.
Winterwerp, J. C., De Groot, M. B., Mastbergen, D. R., and Verwoert, H. (1990). "Hyperconcentrated sand–water mixture flows over flat bed." *J. Hydraul. Eng.*, 116(1), 36–54.
Wolf, F. C. J. (1997). "Hydrodynamics, sediment transport and daily morphological development of a bar-beach system." Doctoral thesis, Dept. of Physical Geography, Univ. of Utrecht, Utrecht, The Netherlands.
Xu, J. (1999a). "Grain-size characteristics of suspended sediment in the Yellow River, China." *Catena*, 38, 243–263.
Xu, J. (1999b). "Erosion caused by hyperconcentrated flow on the Loess Plateau of China." *Catena*, 36, 1–19.